*remote sensing*

MDPI

*Article*

# Comparative Analysis of Earth Observation Methodologies for Irrigation Water Accounting in the Bekaa Valley of Lebanon

**Gabriel Moujabber [1,2], Marie Therese Abi Saab [2,3], Salim Roukoz [4], Daniela D'Agostino [1], Oscar Rosario Belfiore [5] and Guido D'Urso [5,*]**

[1] Department of Sustainable Water and Land Management in Agriculture, Mediterranean Agronomic Institute of Bari, 70010 Valenzano, Italy; gabriel.a.elmoujabber@net.usek.edu.lb (G.M.); dagostino@iamb.it (D.D.)
[2] Department of Agriculture, The School of Engineering, The Holy Spirit University of Kaslik, Jounieh P.O. Box 446, Lebanon; mtabisaab@lari.gov.lb
[3] Climate and Water Unit, Lebanese Agricultural Research Institute, Fanar P.O. Box 90-1965, Lebanon
[4] Ministry of Agriculture, Beirut, Lebanon; salimroukoz@hotmail.com
[5] Department of Agricultural Sciences, University of Naples Federico II, 80055 Portici, Italy; oscarrosario.belfiore@unina.it
* Correspondence: durso@unina.it; Tel.: +39-0812539418

**Abstract:** This study extensively examines the estimation of irrigation water requirements using different methodologies based on Earth Observation data. Specifically, two distinct methods inspired by recent remote sensing and satellite technology developments are examined and compared. The first methodology, as outlined by Maselli et al. (2020), focuses on using Sentinel-2 MSI data and a water stress scalar to estimate the levels of actual evapotranspiration and net irrigation water (NIW). The second methodology derives from the work of D'Urso et al. (2021), which includes the application of the Penman–Monteith equation in conjunction with Sentinel-2 data for estimating key parameters, such as crop evapotranspiration and NIW. In the context of the Bekaa Valley in Lebanon, this study explores the suitability of both methodologies for irrigated potato crops (nine potato fields for the early season and eight for the late season). The obtained NIW value was compared with measured field data, and the root mean square errors were calculated. The results of the comparison showed that the effectiveness of these methods varies depending on the growing season. Notably, the Maselli method exhibited better performance during the late season, while the D'Urso method proved more accurate during the early season. This comparative assessment provided valuable insights for effective agricultural water management in the Bekaa Valley when estimating NIW in potato cultivation.

**Keywords:** evapotranspiration; net irrigation water; earth observation; water accounting; Lebanon; potato; Penman–Monteith



**Citation:** Moujabber, G.; Abi Saab, M.T.; Roukoz, S.; D'Agostino, D.; Belfiore, O.R.; D'Urso, G. Comparative Analysis of Earth Observation Methodologies for Irrigation Water Accounting in the Bekaa Valley of Lebanon. *Remote Sens.* **2024**, *16*, 1598. https://doi.org/10.3390/rs16091598

Academic Editors: Kiril Manevski, Mathias N. Andersen, Junxiang Peng, Juan Antonio Rodríguez Díaz and Konstantinos X. Soulis

Received: 19 February 2024
Revised: 18 April 2024
Accepted: 23 April 2024
Published: 30 April 2024



## 1. Introduction

Agriculture is a crucial sector worldwide for sustainable development, poverty reduction, and food security. Ensuring sufficient food for the increasing population requires developing and intensifying irrigated agriculture, especially in arid and semi-arid regions [1,2]. To meet this demand, there must be a shift toward more productive irrigated agriculture, a category which accounts for 70% of total water use. However, this amount of diverted fresh water does not directly contribute to food production, due to inefficiencies caused by leakages in water distribution systems and insufficient water resources and on-farm water management practices. The United Nations Sustainable Development Goals (SDGs), notably Target 4 of SDG #6, emphasise improving water efficiency in all sectors. In recent years, research on crop "water productivity" and "irrigation water accounting" has illustrated how increasing output or value can improve food security and resource

management. Due to a lack of metering devices and regular monitoring, the amount of water used for irrigation is unknown in many irrigated areas.

Using agro-hydrological models and remote sensing technologies such as Earth Observation (EO), it is possible to identify critical water management areas and evaluate the current and potential use of water for crops. As a result of the suitability of spatial, temporal, and spectral resolutions for agricultural water management applications, European satellites of the Copernicus constellation, including Sentinel-2A (S2A) and Sentinel-2B (S2B), can be used to improve EO to a substantial extent. These new sensor characteristics have led to advanced techniques for estimating crop biophysical parameters for crop models, particularly over large areas, across the growing season with appropriate temporal and spatial resolutions [3,4]. Many studies have presented strategies for integrating crop models with EO-based estimations of crop parameters from freely available data of operational satellite Copernicus Sentinel-2 missions in a variety of applications for irrigation management. These applications consider different types of input variables, such as (i) meteorological data (e.g., air temperature, pressure, wind speed, relative humidity, and solar radiation); (ii) crop biophysical variables, such as the Normalized Difference Vegetation Index (NDVI), leaf area index (LAI), and canopy cover (CC); and (iii) soil hydraulic properties [5–9].

Satellite-based irrigation guidance services were developed to help farmers make better decisions. These services analyse crop water requirements based on climatic conditions and the crop's growth stage [7–9] to estimate evapotranspiration $ET_p$ under "standard" conditions, as defined by the FAO 56 Paper [10,11], i.e., complete availability of water in the soil, and a lack of biotic and abiotic agricultural stressors. In this scenario, crop biophysical characteristics (crop height, albedo, and LAI) and meteorological data determine $ET_p$. Most satellite sensors are typically able to detect crop development utilising visible and near-infrared wavelengths, which do not require knowledge of the soil [9]. Contrastingly, in applications that aim at irrigation water accounting [12], detailed crop and soil water balance models can be implemented together with EO-based input [5,13] to estimate actual evapotranspiration ($ET_a$). Alternatively, surface energy balance has been calculated using EO data in the thermal range to obtain $ET_a$ without requiring precise soil data [5,14]. Recent research has focused on shortwave infrared wavelength data, which are used to derive information about the water status of land surfaces, considering the limitations of thermal range EO in terms of spatial and temporal resolution and issues related to atmospheric corrections sufficiently accurate for deriving land surface temperature from thermal data [15–17]. The availability of accurate radiometric observations with 20 m spatial resolution and acquisitions every five days from S2 platforms has brought new developments in the estimation of $ET_a$ for operational applications in agricultural water management.

In this study, two alternative methodologies, proposed by (i) Maselli et al. (2020) [18] and (ii) D'Urso et al. (2021) [14], for estimating $ET_a$ and net irrigation water use are compared with metered irrigation volumes to assess water accounting, under dry conditions, for potato crops in Lebanon.

This study is part of the international project "Earth Observation Technologies for Irrigation in Mediterranean Environments" (EO-TIME). The EO-TIME project aims to optimise water management in agriculture by combining EO data with Information and Communication Technologies (ICT) and improve irrigation scheme performance regarding technical efficiency, environmental impact, and socioeconomic outcomes in water-scarce regions. The project aims to create integrated systems and services that leverage EO and ICT to manage water resources in river basins, irrigation projects, and individual farms. The purpose is to enable farmers to make intelligent irrigation schedule decisions while considering regional water availability and management decisions.

## 2. Materials and Methods

### *2.1. Characteristics of the Study Area*

In the Bekaa valley of Lebanon, the Upper Litani watershed (33.20–34.10°N, 35.20–0.10°E, Figure 1) is the subject of the study. With irregular precipitation and recurring droughts, the area has a semi-arid Mediterranean climate. The average annual rainfall in the north is about 230 mm, while it is over 850 mm in the western region and 610 mm in the middle valley. The primary irrigated crops in the area include grains, legumes, vegetables, fruit trees, and vines, yet productivity in agriculture is firm despite the region's low levels of precipitation. While spring and summer vegetables are produced under irrigation, winter grains are grown under additional irrigation. Farmers are being forced to use less water for food production due to the growing water shortage in the valley, threatening their livelihoods.

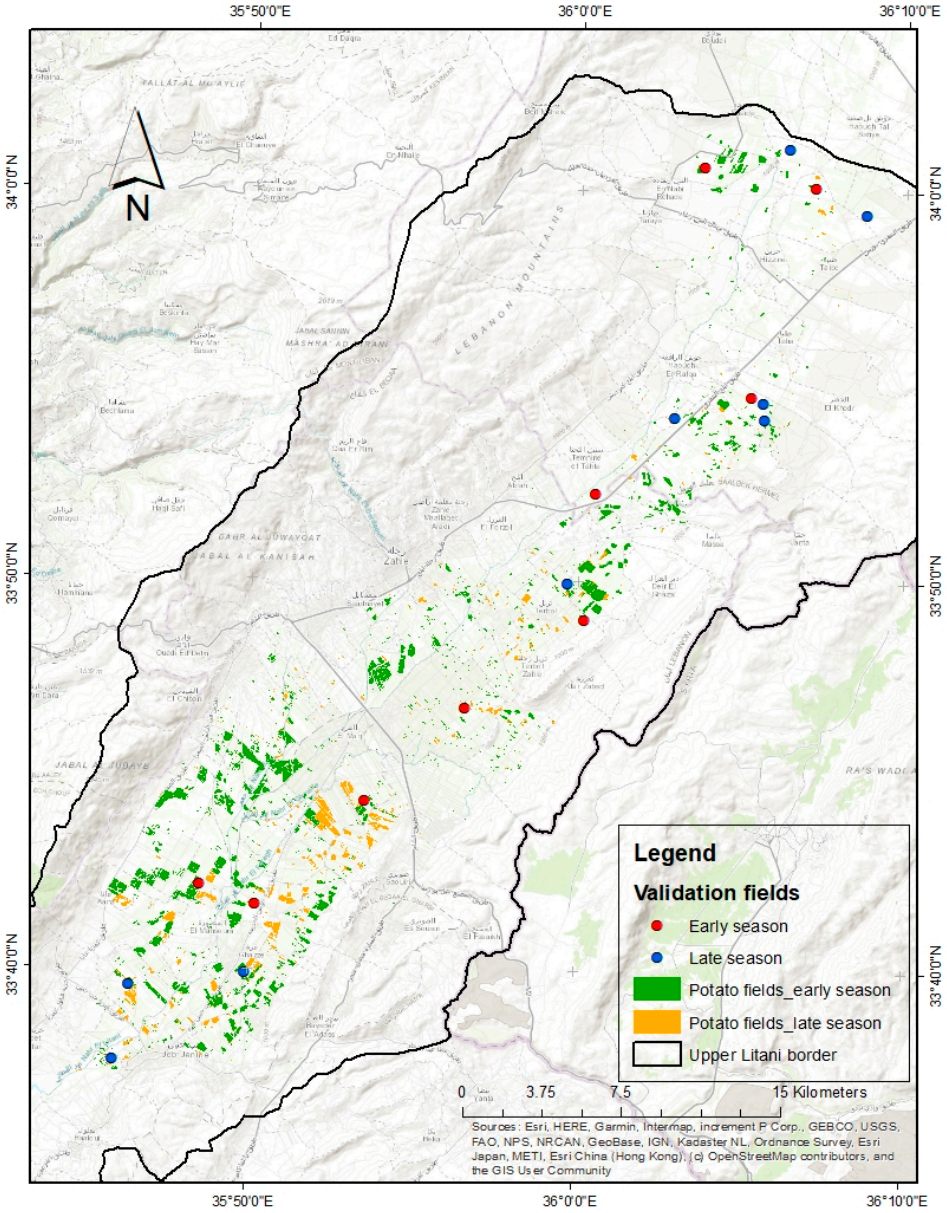


**Figure 1.** Map of Lebanon, showing the geographical position of the Upper Litani and the distribution of the fields grown with potatoes in the early and late seasons of 2020.

The study focused on potato cultivation during the early and late seasons of 2020, given the phenological calendar of potato growth (Table 1). Early-season potato crops

would benefit from rainwater already stored in the soil. At the same time, irrigation water was provided to the crops according to a schedule determined by the farmers' practical experience. The irrigation system farmers use incorporates traditional impact sprinklers spaced at 12 m intervals on a lateral line, with a discharge rate of 1.5 $m^3$/h, and the spacing between the lines is 18 m.

**Table 1.** Phenological calendar of potato in the Upper Litani watershed.

| Crop Type | Sowing Window | Harvest Window |
|---|---|---|
| Potato (early season) | February–March | June–August |
| Potato (late season) | July–August | November–December |

### *2.2. Collected Data Overview*

Field data was collected from 17 potato fields during the early and late seasons in 2020. Information on the growing calendar and the irrigation method used was obtained, and water meters were installed to register the irrigation volumes applied (Table 2). Notably, the net irrigation amounts were estimated from the gross amounts by assuming an efficiency of 70%. Daily meteorological variables (air temperature and humidity, wind speed at 10 m, incoming solar radiation, precipitation P, and reference evapotranspiration $ET_0$) were derived from the fifth Generation of ECMWF Atmospheric Reanalysis of the Global Climate ERA5 [19] (https://cds.climate.copernicus.eu/cdsapp#!/dataset/reanalysis-era5-land?tab=overview, accessed on 10 January 2021).

**Table 2.** Field data used for validation in 2020.

| Season | X | Y | Planting Date | Number of Sprinklers per ha | Sprinkler Application Rate ($m^3$/h) | Net Irrigation Water Use (mm) | | | | Total Net Irrigation Water Use (mm/Season) |
|---|---|---|---|---|---|---|---|---|---|---|
| | | | | | | Until Day 45 | Days 45 to 70 | Days 70 to 100 | Days 100 to 110 | Days 110 to 120 | |
| Early season | 36.062545 | 34.010629 | 15 March | 30 | 1.5 | 19 | 63 | 142 | 38 | 6 | 268 |
| | 36.087906 | 33.912448 | 22 March | 30 | 1.5 | 19 | 57 | 126 | 19 | 6 | 227 |
| | 36.008369 | 33.870860 | 18 March | 30 | 1.5 | 25 | 47 | 95 | 25 | 6 | 198 |
| | 36.119467 | 34.002163 | 1 April | 30 | 1.5 | 28 | 95 | 227 | 38 | 6 | 394 |
| | 35.943419 | 33.778937 | 15 March | 30 | 1.5 | 13 | 57 | 189 | 28 | 6 | 293 |
| | 35.808920 | 33.702613 | 25 March | 30 | 1.5 | 9 | 79 | 198 | 50 | 6 | 343 |
| | 35.892434 | 33.738782 | 25 March | 30 | 1.5 | 19 | 57 | 142 | 25 | 6 | 249 |
| | 35.837074 | 33.694242 | 15 March | 30 | 1.5 | 13 | 79 | 198 | 38 | 6 | 334 |
| | 36.003494 | 33.817086 | 1 April | 30 | 1.5 | 50 | 110 | 221 | 28 | 6 | 416 |
| Late season | 35.995051 | 33.832279 | 1 August | 30 | 1.5 | 28 | 57 | 63 | 0 | 0 | 148 |
| | 35.773305 | 33.659328 | 4 August | 30 | 1.5 | 38 | 57 | 63 | 0 | 0 | 158 |
| | 35.765647 | 33.627283 | 5 August | 30 | 1.5 | 38 | 47 | 28 | 0 | 0 | 113 |
| | 35.832065 | 33.665258 | 1 August | 30 | 1.5 | 63 | 32 | 63 | 0 | 0 | 158 |
| | 36.094344 | 33.902884 | 8 August | 30 | 1.5 | 47 | 16 | 57 | 0 | 0 | 120 |
| | 36.093712 | 33.909883 | 1 August | 30 | 1.5 | 50 | 57 | 63 | 0 | 0 | 170 |
| | 36.048899 | 33.903378 | 17 July | 30 | 1.5 | 28 | 32 | 57 | 0 | 0 | 117 |
| | 36.145770 | 33.990577 | 1 August | 30 | 1.5 | 38 | 32 | 63 | 0 | 0 | 132 |

These data were checked for consistency against those collected from the Tal Amara ground station (35.986899 Long; 33.856866 Lat), which belongs to LARI and is in the Upper Litani watershed. The comparison and the goodness of fit between the cumulative daily values of P and $ET_0$ for the year 2020 extracted from ERA5 and those derived from the Tal Amara weather station are reported in the Supplementary Material (Figures S1 and S2). In addition, the minimum and maximum monthly cumulative values of P and $ET_0$ are provided in Table 3, while the distribution of those parameters within the study area is shown in Figure S3.

**Table 3.** The monthly cumulative values of precipitation P and reference evapotranspiration $ET_0$, as extracted from ERA5 within the study area in 2020.

| 2020 | P (mm) | | $ET_0$ (mm) | |
|---|---|---|---|---|
| **Month** | **Min** | **Max** | **Min** | **Max** |
| January | 83 | 135 | 23 | 28 |
| February | 77 | 141 | 34 | 38 |
| March | 90 | 137 | 64 | 68 |
| April | 35 | 78 | 89 | 97 |
| May | 15 | 42 | 136 | 148 |
| June | 1 | 4 | 150 | 171 |
| July | 0 | 6 | 163 | 185 |
| August | 0 | 5 | 149 | 168 |
| September | 2 | 5 | 124 | 135 |
| October | 2 | 6 | 84 | 90 |
| November | 61 | 97 | 33 | 39 |
| December | 37 | 57 | 27 | 32 |
| Cumulative values in the early season (February to August) | 219 | 413 | 785 | 875 |
| Cum. values in late season (August to November) | 65 | 112 | 391 | 432 |
| Yearly totals | 404 | 713 | 1075 | 1199 |

The twin Sentinel-2A and Sentinel-2B satellites of the European Space Agency provided the Earth Observation images that were utilised to calculate the crop parameters. The nominal revisit time for the Sentinel-2 constellation is five days. Satellite images from Sentinel-2 for each band (Appendix A) for each available day throughout the research period (from the 5th of February to the end of December 2020) were collected. They were downloaded from the ESA website in an ortho-rectified, pre-processed L-2A format (https://sentinel.esa.int/web/sentinel/sentinel-data-access, accessed on 10 January 2021).

The area covered by potatoes in 2020 was obtained from the FAO-WAPOR remote sensing open-access database, accessible through the following link: https://wapor.apps.fao.org/home/WAPOR_2/1, accessed on 10 January 2021.

### *2.3. Prediction Methods for Actual Evapotranspiration and Net Irrigation Water Use*

Two methodologies, derived from existing studies conducted in Mediterranean areas and found in the literature [14,18,20], were used to estimate $ET_a$ and, hence, the net irrigation water use (NIW) of potatoes. NIW is the amount of water farmers apply, calculated from $ET_a$ by considering precipitation and soil water status.

#### 2.3.1. Method (A): NIW Prediction According to Maselli et al. (2020) [18]

The methodology combines meteorological data and the remotely sensed fractional vegetation cover (FVC) [21]. It consists of estimating $ET_a$ and then predicting the NIW through a site water balance approach that accounts for the most recent precipitation events and the rainwater stored in the soil as the sum of the two terms representing transpiration and evaporation:

$$ETa_i = ET_{0i} \times 1.2 \times FVC_i \times (0.5 + 0.5 \times AW_i) + ET_{0i} \times 0.2 \times (1 - FVC_i) \times AW_i \quad (1)$$

In Equation (1) above, the subscript i refers to the generic day, FVC to fractional vegetation cover, and AW to a short-term water stress scalar; 1.2 and 0.2 represent the maximum crop coefficients for herbaceous vegetation and soil. Notably, the daily layers of $ET_o$ were combined with precipitation (Prec) to predict the meteorological water stress scalar (AWi). Then, the FVC was computed from Sentinel images by using the Sentinel Application Platform (SNAP) biophysical processor, which simulates FVC through the application of

an artificial neural network to multispectral Sentinel-2 MSI observations [12,22,23]. The water stress scalar is calculated as follows:

$$AW_i = \frac{\sum_i^{i-29} Prec_i}{\sum_i^{i-29} ETo_i} \quad (2)$$

where the total amount of precipitation (Prec) is bound by ET0, which allows the scalar to range from 0 (with total meteorological water stress) to 1 (no stress).

To account for the irrigated conditions of the spring/summer crops, a modified water stress scalar of day i ($AW_{FVCi}$) was obtained by keeping the maximum of the original AWi and a normalised $FVC_i$ ($FVC_{NORMi}$), calculated as follows:

$$FVC_{NORMi} = \frac{(FVC_i - FVC_{min})}{(FVC_{max} - FVC_{min})} \quad (3)$$

where $FVC_{min}$ and $FVC_{max}$ have been progressively found since the beginning of the dry season. This modification deactivates the water stress scalar (increases it up to 1) when FVC is increasing or close to the seasonal maximum during the summer spring/water stress period. After that, $ET_a$ was computed using Equation (1).

Finally, $NIW_i$ was estimated, reducing the result to account for any precipitation which may have fallen in the same period or accumulated in the soil during the previous weeks. For this, a normalised difference between $AW_{FVCi}$ and AWi was multiplied by $ET_a$.

The algorithm combines indicators of meteorological water stress with temporal FVC variation to dynamically identify the imbalance between the water supplied by precipitation and the level required by the plants, which can serve as the basis for predicting crop irrigation. It is assumed that the daily water needs of irrigated crops can be estimated from the actual transpiration amount over a brief period. The precipitation that may have fallen during the same period or accumulated in the soil over the prior weeks must be reduced from this amount to calculate the actual NIW.

Therefore, this correction will be conducted in two stages. First, since irrigation is not applied during rainy periods, the predicted NIW is set to 0 when the last three days' adequate precipitation determination (i.e., precipitation minus ET0) is favourable. Second, based on the logical framework presented in Maselli et al. [18], which assumes that $AW_{FVC}$ and AW are proportional to the total water and the rainwater transpired by the crop, respectively, an estimate of the contribution of less recent precipitation to soil water storage is calculated. As a result, the normalised difference between the two terms can be utilised to correct the transpired water calculation and be interpreted as a measurement of the water amount provided by irrigation.

The above reasoning leads to the following predictions for irrigation water on non-rainy day i ($NIW_i$):

$$NIW_i = \frac{\sum_i^{i-2} Ta_i}{3} \times \frac{(AW_{FVCi} - AW_i)}{AW_{FVCi}} \quad (4)$$

Figure 2 presents a flowchart of the applied methodology and equations used. All work was conducted using two geographical information system software programs (ESA-SNAP and ArcMap 10.8).

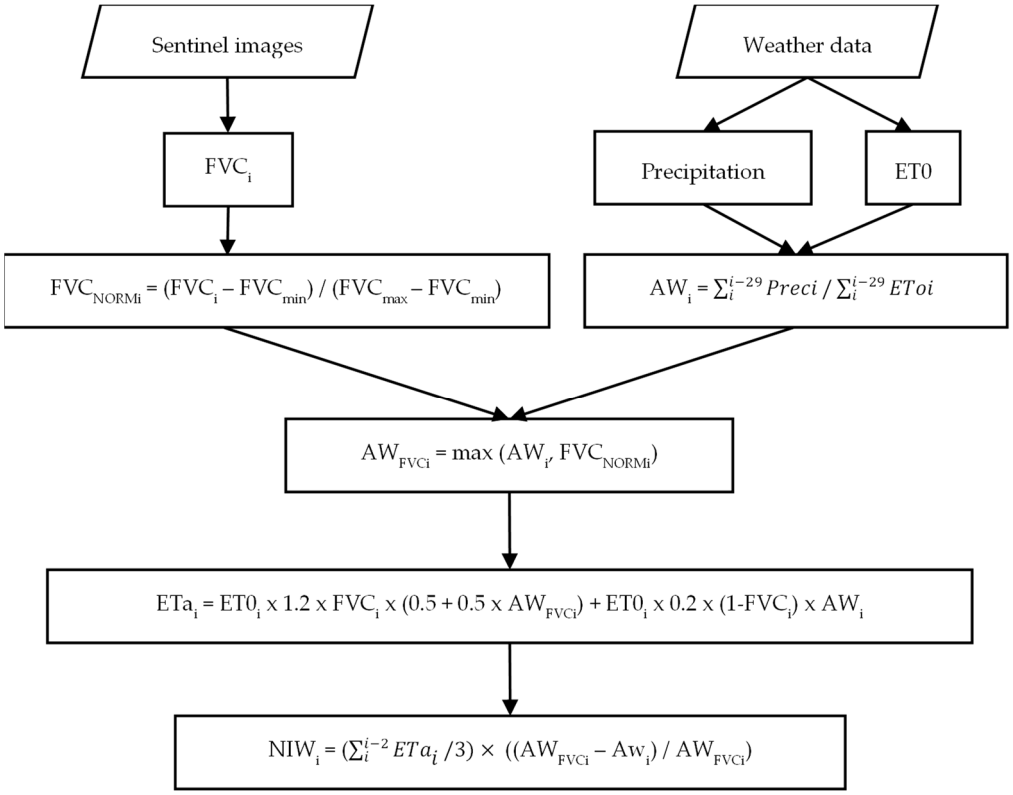


**Figure 2.** Workflow of $NIW_i$ estimation according to method (A), based on Maselli et al. [18].

2.3.2. Method (B): NIW Prediction According to D'Urso et al. (2021) [14]

Estimation of Maximum Evapotranspiration ETp and Effective Precipitation

This methodology used the Penman–Monteith equation model with surface parameters and resistance levels derived from Sentinel-2 data to determine evapotranspiration (ET) according to the so-called "direct approach" in [11]. This strategy has been used in satellite-based advisory services for managing irrigation without using the crop coefficient $K_c$ [24]. In this case, surface parameters derived from Sentinel-2 are used as inputs for calculating ET. In particular, the hemispherical shortwave albedo determines the value of net radiation and the leaf area index (LAI) the value of the bulk stomatal canopy resistance $r_c^s$.

The set of equations is described in detail in D'Urso et al. (2021) [14].

Firstly, the albedo ($\alpha$) approximates the hemispherical and spectrally integrated surface albedo; given the limited spectral resolution of EO data, it is calculated as a weighted sum of surface spectral reflectance derived from the atmospheric correction, with broadband coefficients representing the corresponding fraction of solar irradiance in each sensor band [14]:

$$\alpha = \sum_{\lambda} \omega_\lambda \rho_\lambda \qquad \lambda = 1, 2, \ldots, m \tag{5}$$

where the weighting factors, $\omega_\lambda$, are derived from the equation below using the mean exo-atmospheric solar irradiation in m distinct spectral bands (Appendix B):

$$\omega_\lambda = \frac{E_{SUN,\lambda}}{\sum_{\lambda=1}^{m} E_{SUN,\lambda}} \tag{6}$$

Secondly, the bulk stomatal canopy resistance $r_c^s$ [$sm^{-1}$] is given by

$$r_s^c = \begin{cases} \frac{r_{leaf}}{0.5\ LAI} & \Big| \ LAI \leq 4 \\ \frac{r_{leaf}}{2} & \Big| \ LAI \geq 4 \end{cases} \tag{7}$$

Szeicz and Long [25] first introduced the expression of $r_{sc}$ given in Equation (7), and it was subsequently used in the formulation of the Penman–Monteith equation in the FAO-56 paper [11]. Since, in most instances, only the top half of the crop foliage is constantly contributing to the transfer of heat and vapour, the coefficient 0.5 was added to the denominator. Although the Penman–Monteith approach was initially created for closed canopies, it has been successfully implemented in several hydrological studies when canopy gaps are present, provided that the correct values for resistance levels are included to account for the gap fractions. To achieve this, a numerical inversion of the Penman–Monteith equation [26] can be used to empirically derive the value of $r_{sc}$ using latent heat flux data. The canopy resistance in response to LAI and other environmental factors has been determined using various models [27]. The leaf resistance $r_{leaf}$ in Equation (7), the reciprocal of the leaf conductance, has been the subject of numerous physiological investigations. A minimal value (maximum conductance) of $r_{leaf} = 100\ sm^{-1}$ has been proposed based on measurements of leaves of several species, including trees and herbaceous crops. It is also adopted in the FAO-56 method for crops under standard conditions. This value has been verified based on Fluxnet information on crop and grassland areas [28].

The computation of $ET_p$ using meteorological data and canopy parameters, such as surface albedo, LAI, and crop height, which may be calculated using remote sensing techniques, is made possible by assuming a constant fixed value for $r_{leaf} = 100\ sm^{-1}$. The canopy height $h_c$ is proportional to the values of $d_0$, $z_{0m}$, and $z_{0h}$, using the abovementioned factors [25].

Hence, LAI is the most crucial crop parameter, and its value can be obtained from the spectral observations of Sentinel-2 following the method outlined in the Sentinel-2 Toolbox contained in the ESA package SNAP [3].

Finally, the net irrigation water requirements $NIW_R$ can be determined from the $ET_p$ and effective precipitation $P_{eff}$ [10]; this information is generally used for irrigation scheduling. The difference between effective precipitation and crop-specific potential evapotranspiration is computed as follows:

$$NIW_R = ET_p - P_{eff} \quad if \quad ET_p > P_{eff} \quad otherwise \quad NIW_R = 0\ [\mathrm{mm/d}] \tag{8}$$

Due to its nonlinear relationships with precipitation and potential evapotranspiration, the irrigation requirement may be overestimated or underestimated. Underestimation is just 2.4% worldwide, but can be significant in locations with low net-irrigation needs [11].

The $P_{eff}$ is the percentage of total precipitation (P) directly available to potato crops and which does not runoff. Several factors affect the variation of the $P_{eff}$. The key factors include precipitation characteristics, soil parameters, crop evapotranspiration rates, and irrigation management. However, the soil properties are parameters which are not used in the $P_{eff}$ calculations. Precipitation efficiency is highly influenced by absorption and retention qualities, such as water release and movement. The $P_{eff}$ is extremely difficult to determine; however, the United States Department of Agriculture (USDA) soil conservation approach is used to determine the $P_{eff}$ using the following formulas:

$$P_{eff} = \frac{P(4.17 - 0.2P)}{4.17} \quad if \quad P < 8.2\ mm/day \tag{9}$$

$$P_{eff} = 4.17 + 0.1P \quad if \quad P \geq 8.2\ mm/day \tag{10}$$

From $ET_p$ to $ET_a$ by Use of SWIR Observations

When there are no restrictions on water resource availability, irrigation applications are generally abundant, so $ET_a = ET_p$, i.e., no crop water stress occurs. In this latter case, $NIW = NIW_R$, meaning that irrigation requirements can be of the same magnitude as actual net irrigation water use. Diversely, in dry and water-scarce areas, where water resources can be limited for long periods during the growing season, the assessment of net irrigation water use requires that soil and plant water status be considered. Although extensive

research has been conducted into detecting soil water content using remote sensing [29], there are still significant constraints for applications at the field scale regarding spatial and temporal resolution and vegetation cover. Vegetation water indices have been established to complement the widely used normalised difference vegetation index, NDVI, and it has been demonstrated that the shortwave infrared signal is sensitive to vegetation water content [30]. The possibility can be considered that the values of surface resistance levels in the ET calculations are modulated depending on the water status of the soil and the canopy water status, evaluated by using a spectral index based on the shortwave infrared observations of Sentinel-2 [14]. Sadeghi et al. [15] suggested a physically based trapezoidal space called the "Optical TRApezoid Model" (OPTRAM) for estimating the water status of the soil and canopy ensemble. The idea is based on the distribution of pixels in the STR-NDVI space, where STR stands for shortwave infrared transformed reflectance:

$$STR = \frac{(1-\rho_{SWIR})^2}{2\rho_{SWIR}} \tag{11}$$

The distribution of STR and NDVI for a crop surface generally falls within trapezoids (Figure 3a), whose borders represent limited wet and dry conditions.

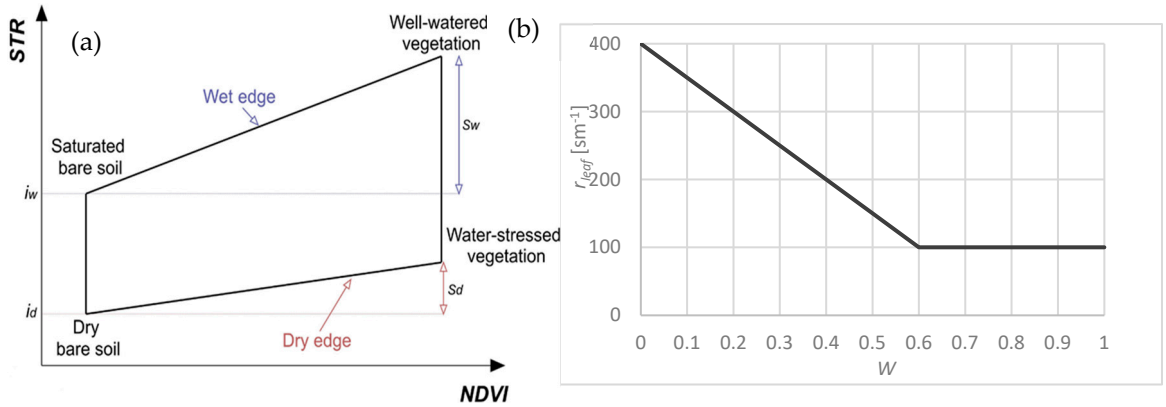


**Figure 3.** (**a**) NDVI-STR space for the suggested substrate and leaf stomatal resistance regulation in the OPTRAM approach and (**b**) variation of the leaf resistance $r_{leaf}$ with the water index W, as taken into consideration in this study (literature reference in the text).

Plotting the values of pixels of NDVI and STR over a given area for various dates (under various climatic circumstances) allows us to determine the limits of this domain. The two limits in the (STR, NDVI) domain are determined by using the following equations to establish the slope and intercepts for dry ($s_d$, $i_d$) and wet ($s_w$, $i_w$) edges:

$$STR_d = i_d + s_d NDVI \tag{12}$$

$$STR_w = i_w + s_w NDVI \tag{13}$$

According to Sadeghi et al. [16], a linear relationship exists between soil saturation degree, W (0 for arid soil and 1 for saturated soil), and STR, resulting in:

$$W = \frac{STR - STR_d}{STR_w - STR_d} \tag{14}$$

When using band 12 of the Sentinel-2 data, it has been demonstrated that W is a proxy for the degree of soil water saturation, with significant correlation with the measured soil water content ($R^2 > 0.8$) [16]. However, in this method, we propose to employ W only as an index to modulate the soil and canopy resistance levels $r_s^s$ and $r_{leaf}$ between wet conditions (W = 1) and dry conditions (W = 0), corresponding to their lower and higher limits. Before the water index falls below a predetermined threshold $W_s$, the value of $r_{leaf}$ is maintained,

constant at $r_{leaf,\ min}$; after that, $r_{leaf}$ is linearly increased up to $r_{leaf,\ max}$ (Figure 3b). Although validating the resistance function shown in Figure 3 would be rather tricky, the fundamental assumptions align with comparable consolidated parameterisations, such as those for root water uptake [31]. With limit values of 2000 and 500 $sm^{-1}$, the substrate resistance $r_s{}^s$ is thought to be inversely linked to W over the entire range of 0 to 1.

This approach increases the value of $r_{leaf}$ to be used in Equation (7), used to calculate ETa using the Penman–Monteith equation. The methodology has been tested in irrigated vineyards in California [14] using Eddy Covariance measurements, and other validation experiments are currently being carried out for different types of crops.

### *2.4. Data Evaluation and Validation*

The predicted NIW was assessed by comparing it with the ground measurements collected from the 17 potato fields during the early and late seasons in 2020. The statistical indicators used were RMSEs.

The root mean squared error (RMSE) describes the average difference between simulation outputs and experimental data, as described below:

$$RMSE = \left[ N \sum_{i=1}^{N} (P_i - O_i)^2 \right]^{0.5} \quad (15)$$

where N is the number of pairs of observed/measured ($O_i$) and predicted/simulated ($P_i$) data.

## 3. Results

### *3.1. Crop and Surface Parameters Derived from Remote Sensing*

The following results are based on the remote sensing data extracted from Satellite imagery. In Figure 4, the trends for the potatoes grown showed a peak of FVC in May–June, followed by, for most fields, a rapid decrease in the dry summer period until the end of the season before harvesting at the beginning of August. The Mediterranean natural grasslands are known for their FVC decrease from spring to summer, which results in a significant NIW estimate for this period.

Figure 4a shows some different FVC variations of potato crops in the early-season validation fields. Figure 4 shows different FVC variations of potato fields during the late season, with a peak in early October followed by a slight decrease in the moist fall period, extending, for most fields, until the end of the season before harvesting at the end of November. The Mediterranean natural grasslands are known for their steady, slow FVC decrease from October to November.

The temporal plots of NDVI in Figure 5, and of the hemispherical surface albedo in Figure 6. NDVI trends for early- (a) and late-season (b) potato validation fields. show surface reflectance coefficients from Sentinel-2. The values in these plots represent the values of NDVI and surface Albedo for the early- and late-season fields, respectively. Similarly to FVC trends, NDVI values increase gradually at the beginning of both seasons, to reach the maximum halfway each season, and then NDVI starts decreasing towards the harvest period.

The fluctuations in NDVI values during the growing season of a potato crop are typically a result of the complex interactions between the potato plant physiology, environmental conditions, and management practices used by each farmer during the season.

The albedo ($\alpha$) is calculated as a weighted sum of surface spectral reflectance, with broadband coefficients representing the corresponding fraction of solar irradiance in each sensor band, as described in Equation (6).

The leaf area index (LAI) is the most crucial crop parameter when calculating evapotranspiration using the P-M combination equation approaches. For Sentinel-2, LAI values were obtained by following the steps outlined in the Sentinel-2 Toolbox contained within the ESA package SNAP [32].

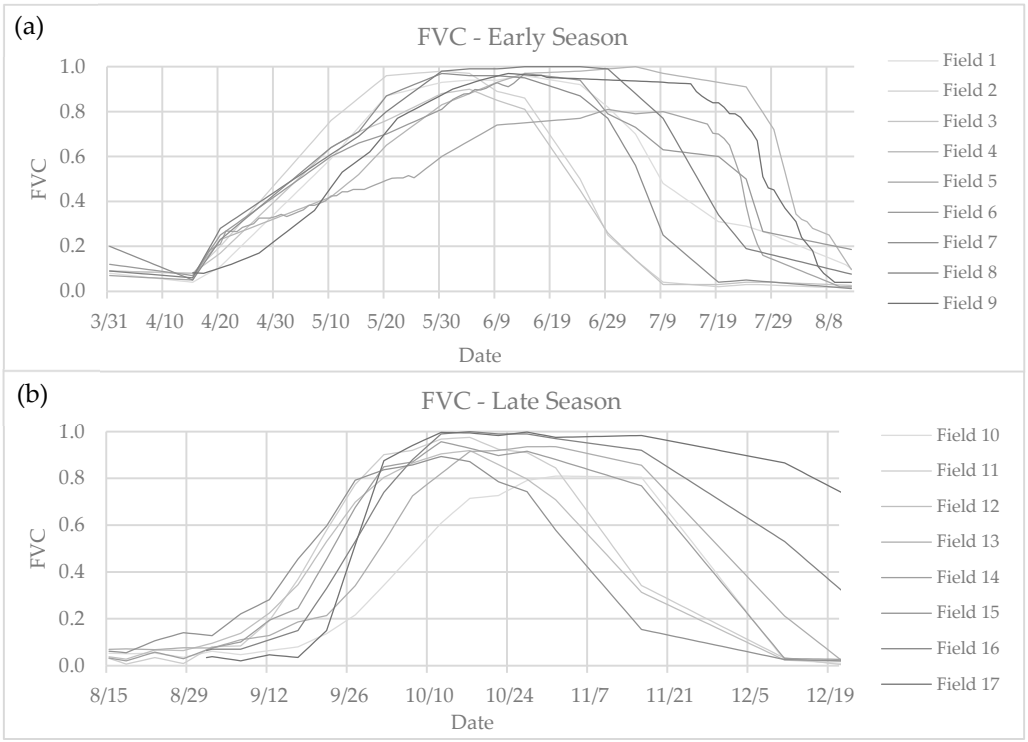


**Figure 4.** FVC trends for early- (**a**) and late-season (**b**) potato validation fields.

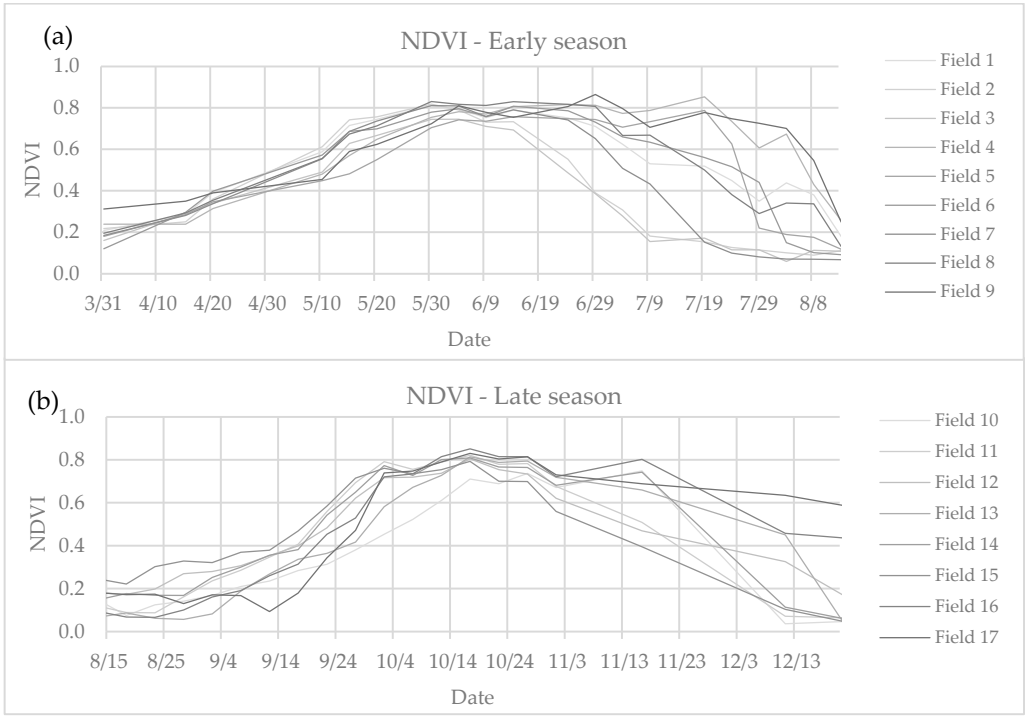


**Figure 5.** NDVI trends for early- (**a**) and late-season (**b**) potato validation fields.

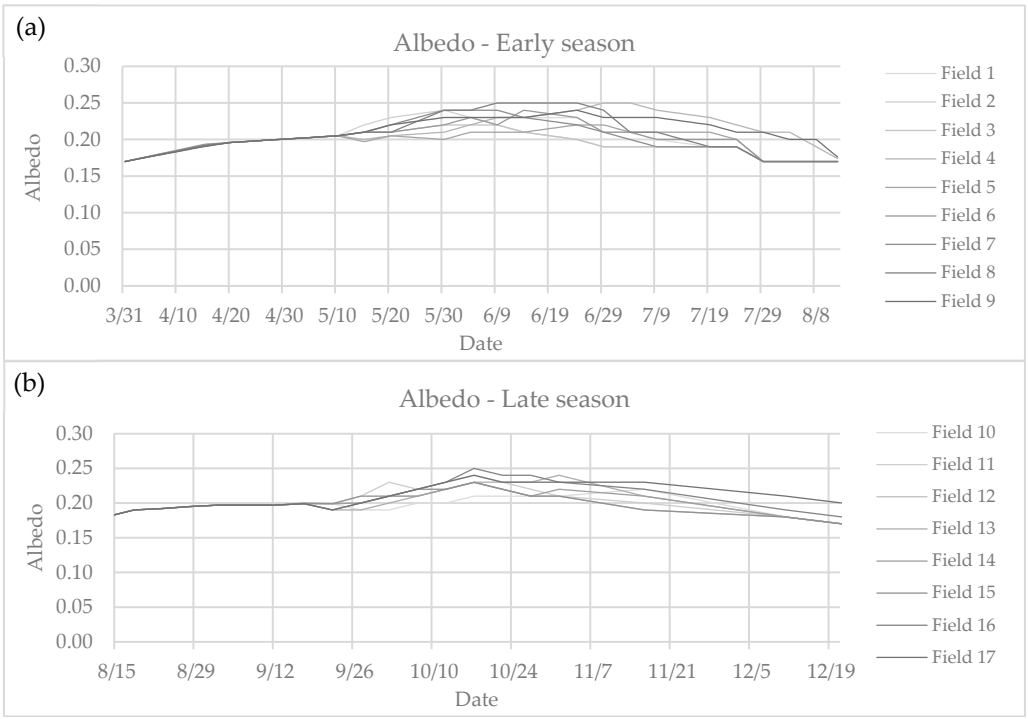


**Figure 6.** Albedo trends for early- (**a**) and late-season (**b**) potato validation fields.

The trends in Figure 7 show a fundamental temporal pattern in LAI from Sentinel-2. Because some of the leaves on the potato plants begin to deteriorate and fall off as they grow, the LAI for the potato crop declines in June for early season and October for the late season. In general, both seasons and the 17 chosen fields exhibit significant variations in the Sentinel-2 LAI values.

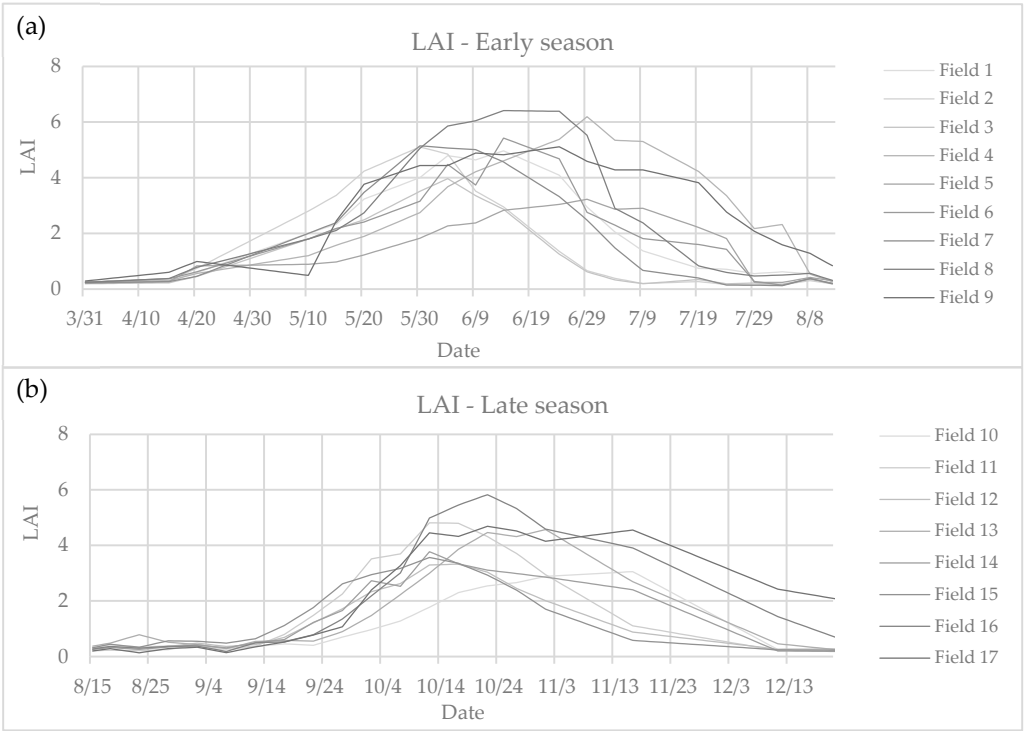


**Figure 7.** LAI trends for early- (**a**) and late-season (**b**) potato validation.

There are several reasons why LAI varies throughout the potato crops. These include variances in crop management techniques like fertilization and insect control. LAI can also be influenced by field history, which includes past crop rotations, tillage methods, and soil management. By being aware of these variables, farmers can adjust their management tactics to maximize LAI and, as a result, raise the quantity and quality of potatoes produced in each field.

The "shortwave infrared transformed reflectance" (STR) in Equation (11) has been calculated using the surface reflectance in Band 12 of Sentinel-2. The graphs in Figure 8 show that, theoretically speaking, the values of STR based on Band 12, with a central wavelength of 2190 nm, have an interval from 0.85 to 5.8. This shows Band 12 of Sentinel-2 to have good sensitivity for this study's objects of observation.

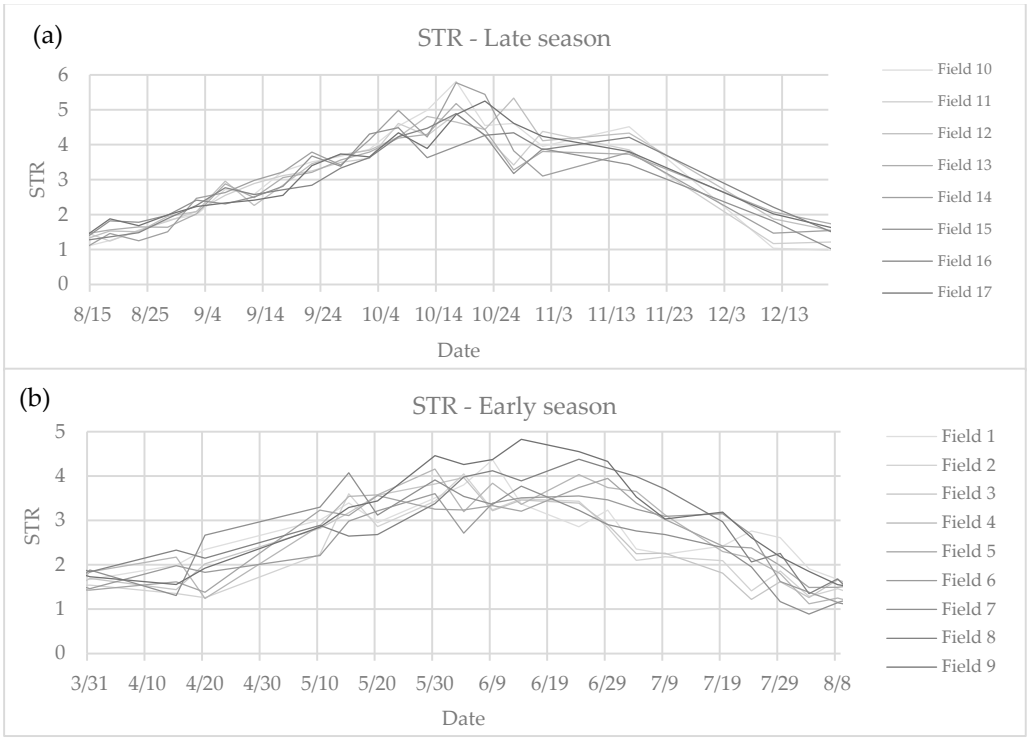


**Figure 8.** STR trends for early- (**a**) and late-season (**b**) potato validation fields.

The value of STR increases following the sizeable amounts of irrigation applied in May (early season) and October (late season), and then the amount drops towards the end of each season. The lower STR values in the time series figure further highlight that fields 2, 3, and 7 (early season) correspond to lower irrigation levels.

Variations in SWIR transformed reflectance in potato crop fields are caused by several variables, such as plant health, nutrient content, soil qualities, environmental factors, agricultural practices, and the sensitivity of data processing and instrumentation. The reflectance characteristics of the soil surface and crop canopy, which are observable in the SWIR spectrum, vary because of changes in these parameters.

### *3.2. NIW Prediction According to Method (A)*

#### 3.2.1. Meteorological, FVC, and NIW Patterns in 2020

In Figure S1, the precipitation and reference evapotranspiration ($ET_0$) distributions are shown for the year of the study, 2020. Precipitation is abundant in the winter and fall periods, from January to early April (400–450 mm) and from late October until the end of December (150–200 m) (the beginning and end of the year). In contrast, the spring and summer precipitation levels combined are modest (80–100 mm). On the opposite side, $ET_0$ is low in winter (100–110 mm) and fall (60–200 mm) and high in spring (270–390 mm)

and summer (460–540 mm). The dry season begins in early May and lasts until October; however, water stress occurs from June to September due to these weather patterns.

The following results are based on the ERA5 land dataset, as extracted. In Figures 9 and 10, two FVC and NIW images, from both the early and the late seasons of the potato fields, are displayed. For each season, the first image is extracted at the beginning, and the second is extracted at the peak period (depending on the availability of the Sentinel-2 images). As evident in these images below for the early season, the NIW values are low at the beginning of the season, ranging between 0–2 mm/day, and increase gradually with the growth of the potato crops throughout the season to reach 6–8 mm/day during the peak in June.

The total NIW predicted over the study area equals 3433 mm for the selected fields, 2601 mm for the early season, and 832 mm for the late season. This variation can be explained by the varying meteorological conditions throughout the year.

As previously mentioned, $ET_0$ was lower in the late season than in the early season; the water deficit is equal to the difference between ET0 and precipitation (i.e., 283 mm in the early season and 400 mm in the late season, or a relative decrease of 29%). This different meteorology presumably led to more stressed conditions for the early-season potato crop and to a consequent pressure to increase irrigation during that period.

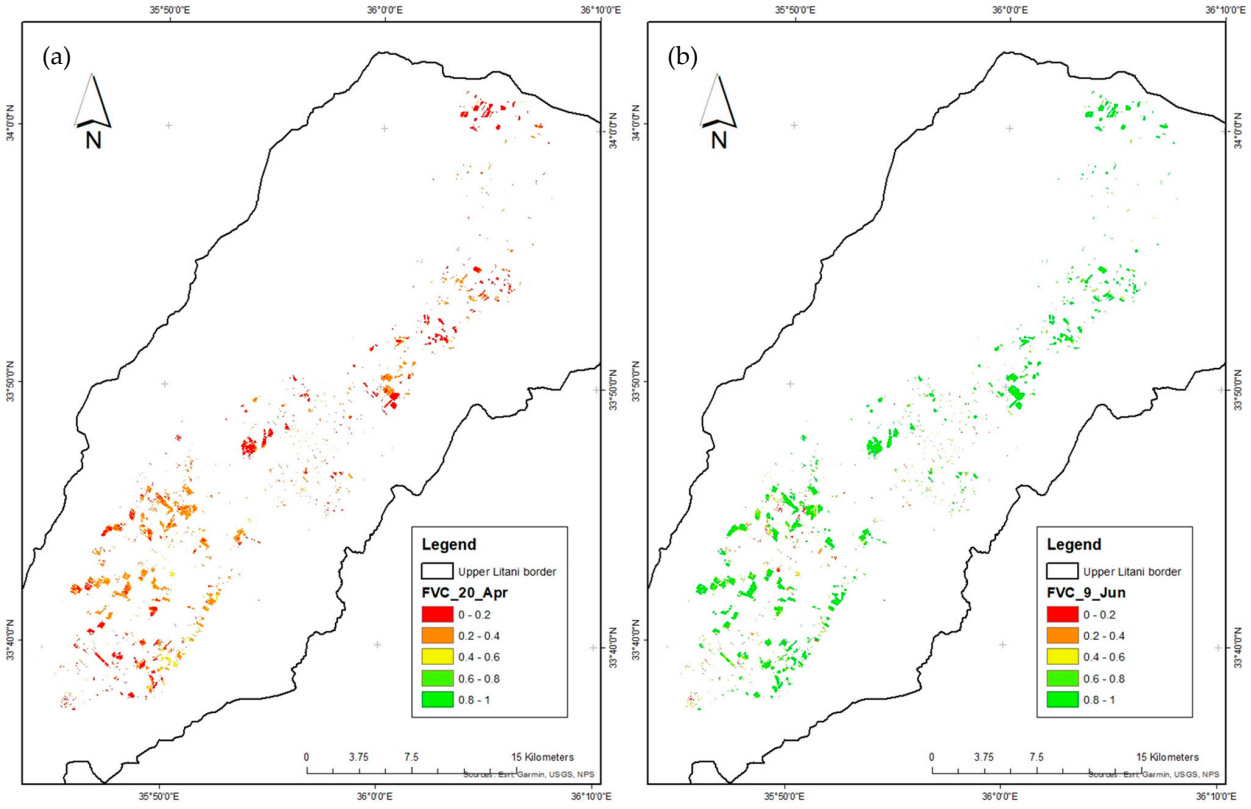


**Figure 9.** *Cont.*

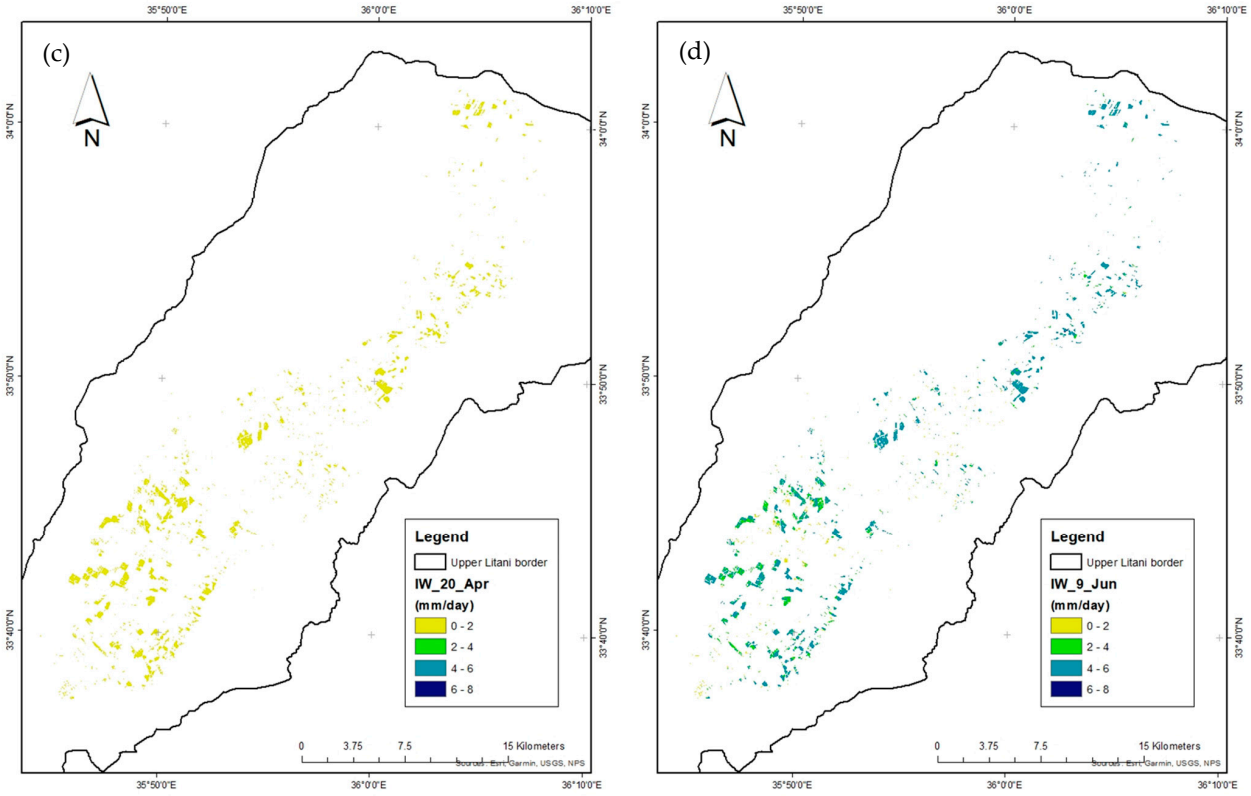


**Figure 9.** Examples of Sentinel-2 FVC images at the beginning ((**a**)—20 April) and peak period ((**b**)—9 June) of the early season, and maps of NIW as predicted by the described procedure at the beginning ((**c**)—20 April) and peak period ((**d**)—9 June) of the early season of 2020.

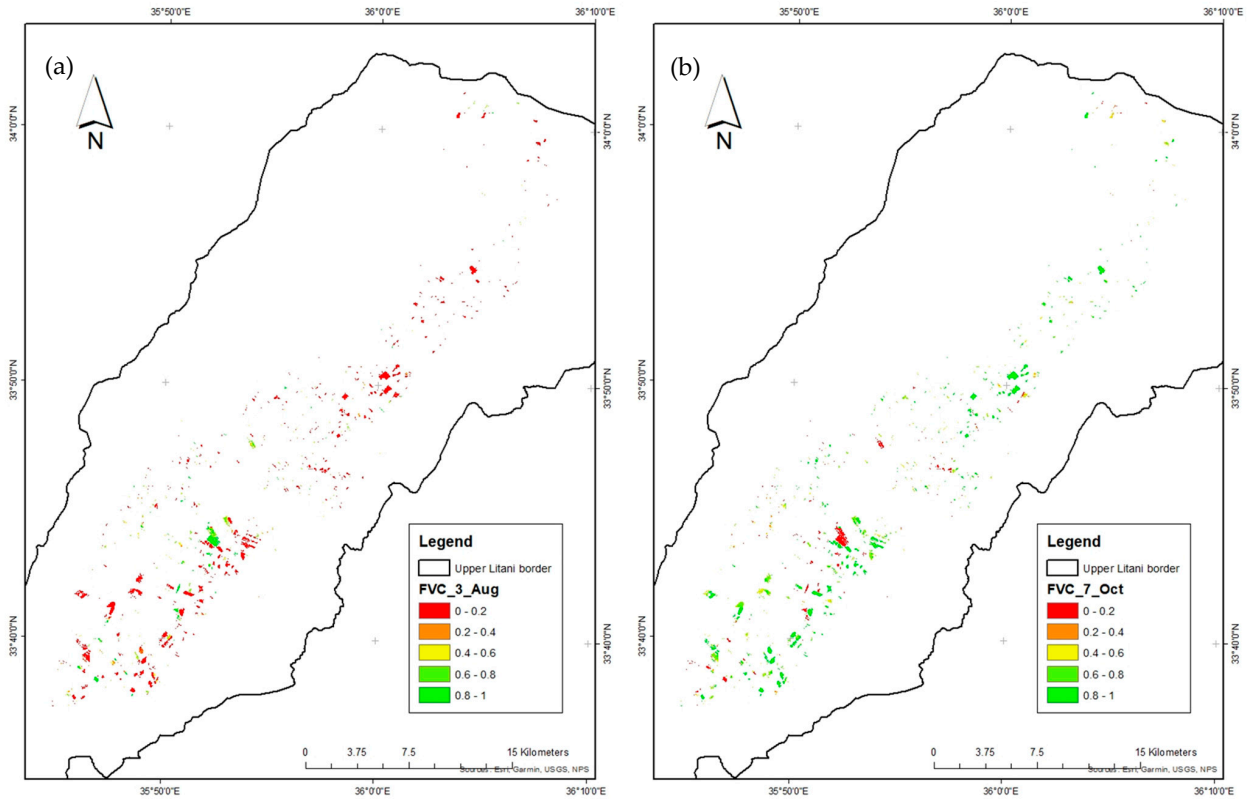


**Figure 10.** *Cont.*

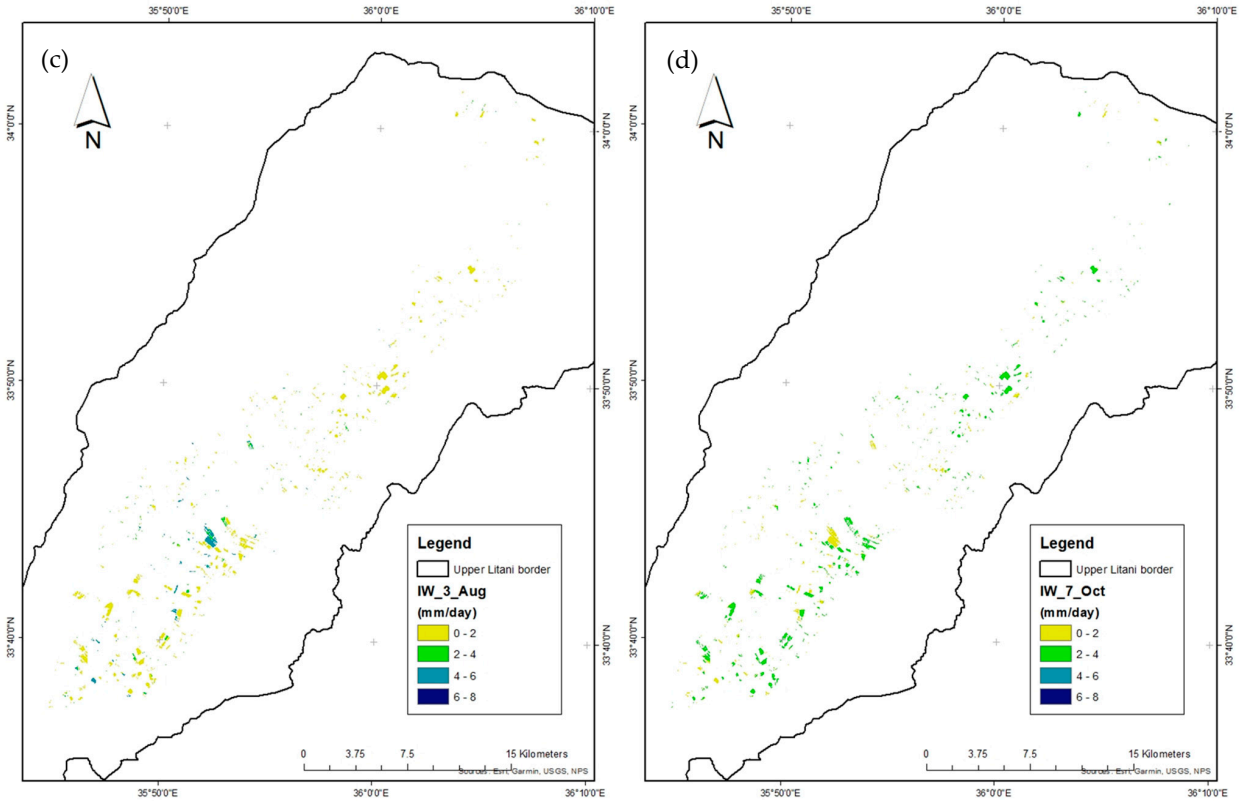


**Figure 10.** Examples of Sentinel-2 FVC images at the beginning ((**a**)—3 August) and peak period ((**b**)—7 October) of the early season, and maps of NIW as predicted by the described procedure at the beginning ((**c**)—3 August) and peak period ((**d**)—7 October) of the early season of 2020.

#### 3.2.2. Trends of Estimated FVC, $ET_a$, and NIW in Validation Fields

In Figure 11, the trends of the potatoes grown showed a peak of FVC and $ET_a$ in May–June, followed by a rapid decrease, for most fields, in the dry summer period until the end of the season before harvesting at the beginning of August. Because of this trend, $ET_a$ is high until July. The Mediterranean natural grasslands are known for their FVC decrease from spring to summer, which results in a significant NIW estimate in this period.

The trend of potato crop $ET_a$ mostly matches that of NIW; however, throughout the growing cycle, when precipitation contributes to soil water recharge and crop transpiration, the latter is lower than $ET_a$.

Figure 12 shows different FVC, Eta, and NIW variations of potato fields during the late season, with, for most fields, a peak in early October followed by a slight decrease in the moist fall period until the end of the season, before harvesting at the end of November.

Because of this trend, $ET_a$ is high throughout October. In the late season of potato cultivation, NIW tends to be lower than in the early season. This phenomenon can be attributed to the fact that precipitation gradually replaces the need for irrigation as the season progresses, reducing the demand for additional watering. The Mediterranean natural grasslands are known for their steady, slow FVC decrease from October to November, which results in a low NIW estimate for this period.

The trend of potato crop ETa mostly matches that of NIW; however, throughout the growing cycle, when precipitation contributes to soil water recharge and crop transpiration, the latter is lower than $ET_a$.

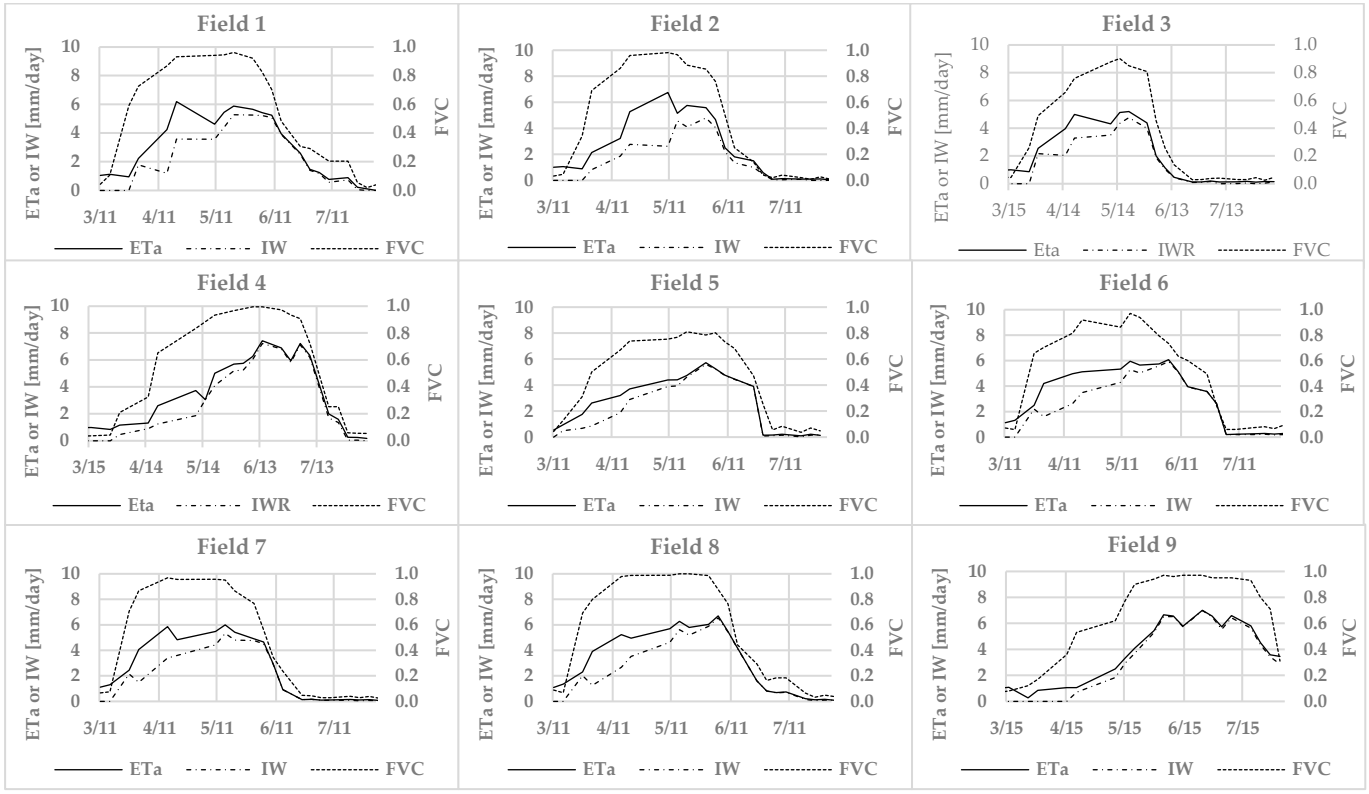


**Figure 11.** FVC, $ET_a$, and NIW trends for each early-season potato validation field.

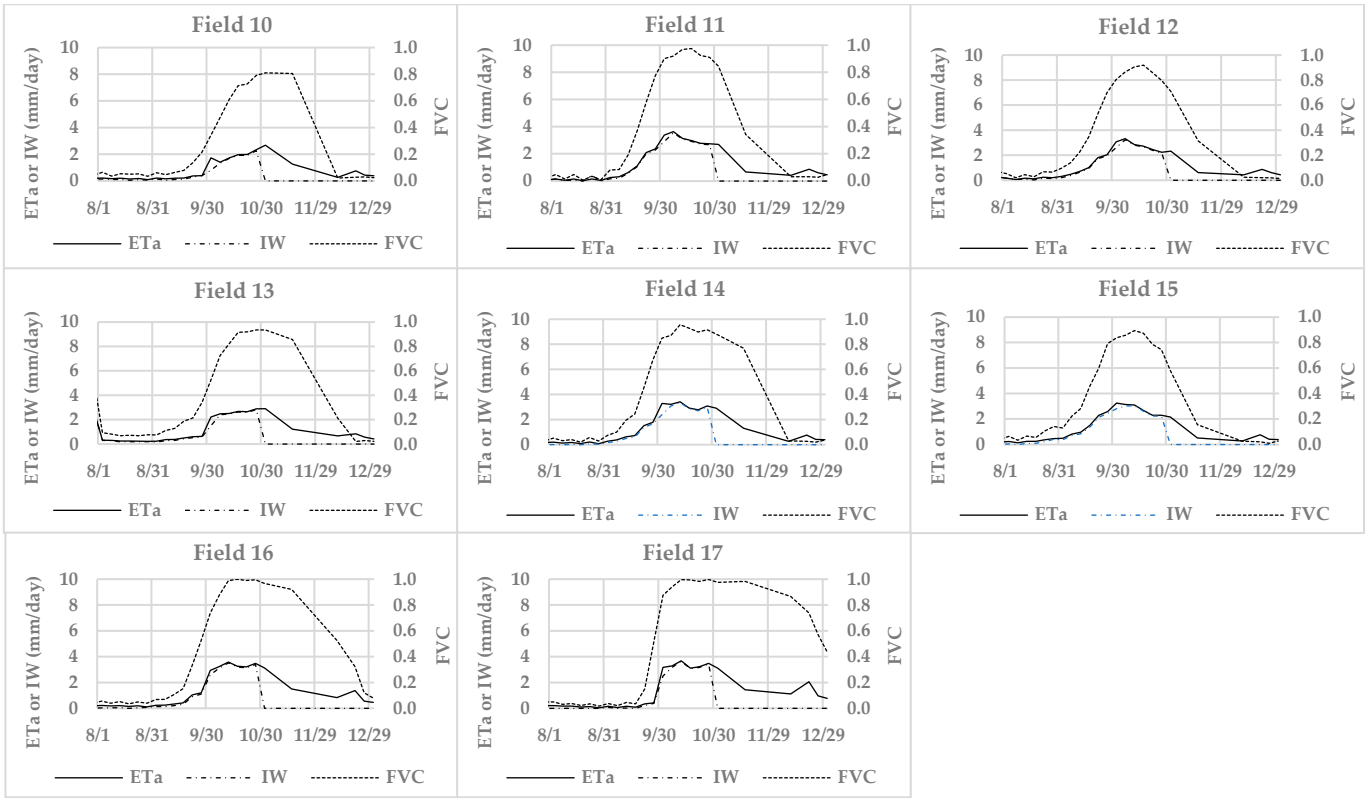


**Figure 12.** Trends for the FVC, $ET_a$, and NIW of each late-season potato validation field.

### *3.3. NIW Prediction According to Method (B)*

The ERA5 dataset used in this method encompasses a comprehensive array of meteorological variables, including temperature, precipitation, wind speed, relative humidity, pressure, radiation, evaporation, cloud cover, and surface variables such as temperature and solar radiation, in addition to the crop and surface parameters mentioned in Section 3.1. The NDVI-STR domain has been plotted by considering the average pixel values in the Sentinel-2 images subset covering each of the selected 17 fields in the Upper Litani watershed to determine the leaf resistance $r_{leaf}$ by using the method in Section From $ET_p$ to $ET_a$ by Use of SWIR Observations. It was decided not to calibrate the resistance as a function of the water index W but to use the standard values described in Section 2, i.e., Figure 3, which should cover various potential scenarios.

The plot shown in Figure 13 was created using the entire collection of Sentinel-2 images provided in Appendix A. The NDVI-STR observed across a particular scene portion is considered to determine the domain borders specific to a given location. The current study uses visual inspection to distinguish between dry and wet borders. This is not a significant flaw in the methodology because the pixel distribution on the NDVI-STR domain has a constant shape for every given location and time, regardless of the surface and weather conditions. Oversaturated or darkened pixels are those that are excluded over the wet edge. Due to difficulties in delineating the dry and wet boundaries, the oversaturated pixels should be eliminated from the NDVI-STR domain.

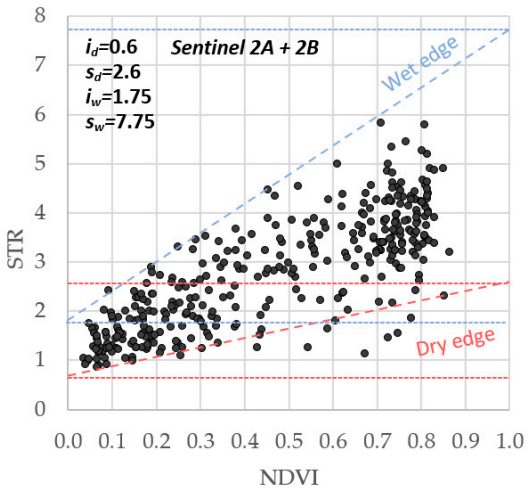


**Figure 13.** NDVI-STR domain for the Upper Litani watershed, extracted from the time series of 2020 Sentinel-2 images (Appendix A). Wet and dry edges are shown with dashed lines. The parameters of Equations (12) and (13) are indicated in the right corner.

A recent study defined the boundaries of the NDVI-STR domain in alternative ways; this aspect may need to be reviewed to improve the methodology [17]. The intercepts and slope values for the lines representing the wet and dry edges of the Upper Litani watershed are shown in Figure 13. Based on these data, the value of W in Equation (14) has been calculated for each date.

In Figure 14, the values of water index W are derived using Equation (14). It is possible to notice in the early season a slight increase in W at the beginning, lasting until the halfway point of the season, with values ranging between 0.2–0.4, meaning that the crops are under stress, and then a rapid increase with the intensification of irrigation applications, associated with values between 0.60–0.78 from the beginning of June. The value of W in this last period decreases again towards the end of the season, along with the reduced amount of irrigation. Similar behaviour has been observed in all nine fields. For the late season, a similar pattern has also been observed, compared with the early season, with a slight difference in which, in the last half of the season, the W value was stable, ranging between 0.4–0.5 after decreases in the amount of irrigation, which were caused by the amounts of

precipitation in the previous two months of the year, during which the crop was rainfed. Similar behaviour has been observed in all eight fields.

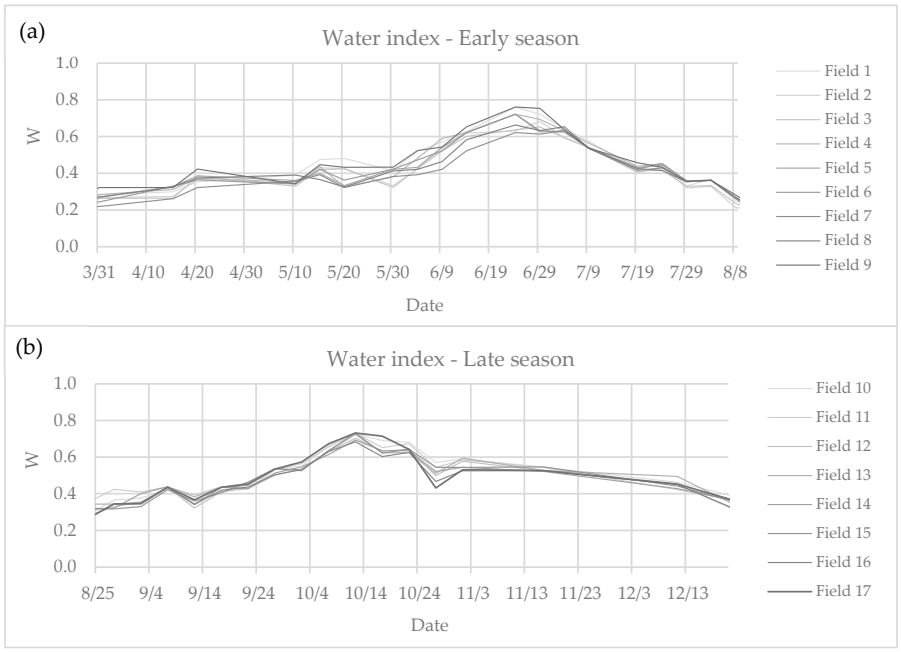


**Figure 14.** Temporal series of Water index W for early- (**a**) and late-season (**b**) potato validation fields.

The leaf resistance $r_{leaf}$ (Figure 15a) starts to decrease in early July for the early season due to the level of irrigation water applied, in conjunction with shortwave infrared transformed reflectance STR, as illustrated in Figure 8a, with a value of 260–400 $sm^{-1}$ in June, decreasing rapidly from early July to its minimum value of 100 $sm^{-1}$ at the end of July, when W is less than 0.6 (Figure 3b). On the other hand, for the late season, $r_{leaf}$ (Figure 15b) starts to decrease in the middle of October (late season), with a value of 250–400 $sm^{-1}$ in October, declining rapidly from early November to its minimum value of 50 $sm^{-1}$ at the end of December.

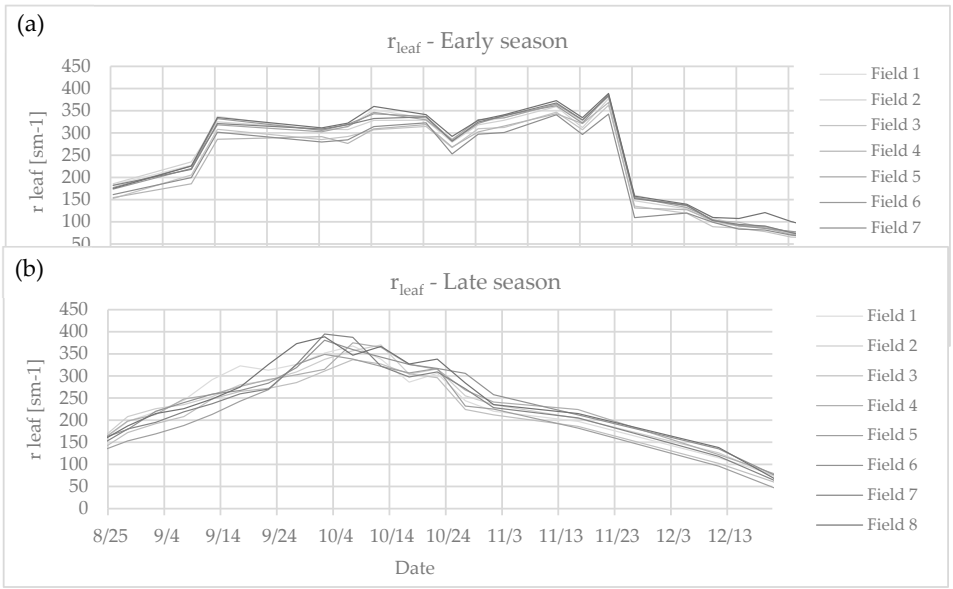


**Figure 15.** Temporal series of leaf resistance $r_{leaf}$ in the Peman–Monteith Sentinel-2 models modulated by using the OPTRAM approach satellite for early- (**a**) and late-season (**b**) potato validation fields.

### *3.4. Data Evaluation and Validation*

Table 4 reports the NIW values collected from the fields and calculated using methods (A) and (B) for each season.

**Table 4.** Comparison of NIW [mm/season] data collected from the field with data estimated from Maselli's and D'Urso's methodologies.

| Season | Field Number | NIW_Field Data | NIW_(A) | NIW (B) |
|---|---|---|---|---|
| Early season | 1 | 268 | 279 | 256 |
| | 2 | 227 | 203 | 188 |
| | 3 | 198 | 177 | 158 |
| | 4 | 394 | 383 | 380 |
| | 5 | 293 | 262 | 222 |
| | 6 | 343 | 321 | 278 |
| | 7 | 249 | 242 | 228 |
| | 8 | 334 | 316 | 309 |
| | 9 | 416 | 418 | 393 |
| Late season | 10 | 148 | 125 | 136 |
| | 11 | 158 | 108 | 139 |
| | 12 | 113 | 100 | 127 |
| | 13 | 158 | 107 | 145 |
| | 14 | 120 | 99 | 127 |
| | 15 | 170 | 109 | 145 |
| | 16 | 117 | 97 | 128 |
| | 17 | 132 | 86 | 140 |

Table 5 displays the root mean square error (RMSE) values for both methodologies compared to the field data for potato net irrigation water use (NIW).

**Table 5.** RMSE statistical results for NIW, between field data and methodologies (A) and (B), as calculated for early and late potato seasons.

| | RMSE_Method (A) (mm) | | RMSE_Method (B) (mm) | |
|---|---|---|---|---|
| **Season** | **Early Season** | **Late Season** | **Early Season** | **Late Season** |
| Until day 45 | 20 | 33 | 20 | 17 |
| Days 45 to 70 | 27 | 23 | 14 | 15 |
| Days 70 to 100 | 37 | 20 | 61 | 28 |
| Days 100 to 110 | 19 | 0 | 15 | 3 |
| Days 110 to 120 | 22 | 0 | 13 | 1 |
| Seasonal total | 18 | 40 | 39 | 15 |

The root mean squared error RMSE mentioned in Section 2.4 was computed for specific Sentinel-2 satellite data acquisition dates, as shown in Table 5.

Figure 16 shows the NIW comparisons for both methodologies with the field data. In comparing the NIW of potato crops between two methodologies, it is evident that in the early season Method A exhibits higher irrigation volumes during the early stages of the growing season, whereas Method B distributes irrigation more evenly throughout the entire season.


**Figure 16.** NIW comparison between field data and method A (Maselli) and method B (D'Urso) for early-season validation fields.

Contrary to the previous scenario, in this comparison of NIW for late-season potato crops (Figure 17), Method B demonstrates higher irrigation volumes during the early stages of the growing season, while Method A distributes irrigation more heavily towards the late stages of growth.


**Figure 17.** NIW comparison between field data, method A (Maselli) and method B (D'Urso) for late-season validation fields.

## 4. Discussion

Maselli's proposed methodology (A) is based on the primary assumption that the NIW corresponds to the crop water requirements not covered by precipitation, which suggests that local farmers are experienced in water resource management. This assumption is reasonable in the study area since most farmers irrigate carefully due to the high cost of obtaining water from the most common sources, mainly deep wells. Such an expectation is reinforced by recent experimental data, which show that the NIW by local farmers is close to the level required by the cultivated crops. Saving water is also a significant motivation for this study, as farmers use sprinklers to irrigate their potato crops, which justifies the current decision to consider $ET_a$ for NIW prediction.

This method predicts the NIW necessary for maintaining plants under the reported greenness conditions, which may not always correspond to complete water satisfaction. The studied crop may have an incomplete FVC, and the water stress scalar may be partially deactivated, limiting the projected $ET_a$ in the presence of mainly dense or green plants [20].

In common practice, this approach provides a lower-limit estimate of NIW, which can be exceeded unintentionally or purposely.

From a functional point of view, the method employs a previously proposed $ET_a$ estimation algorithm that assumes that crop evapotranspiration can be affected by both short- and long-term water stress, with the first being accounted for by a meteorological scalar and the latter by a possible FVC decrease [21]. Since the computation of the meteorological scalar was initially based on precipitation estimates, it must be corrected in situations where there is an additional water supply, i.e., in irrigation conditions. The correction, which is entirely presented and tested in Maselli et al. [20], is based on the identification of temporal divergences between meteorological water stress and FVC, i.e., of cases in which FVC is increasing or very close to the seasonal maximum during periods of intense water stress. This concept was proposed by Ozdogan and Gutman [2], who demonstrated that combining meteorological water stress indicators and FVC data is highly beneficial for detecting irrigated croplands in regions with explicit summer water limitations. Long-term meteorological water stress usually leads to persistent soil water scarcity in rainfed ecosystems [33]. This is not the case when irrigation is applied. The two situations are manifested in diverging green biomass and NDVI evolutions, i.e., decreasing or increasing trends, providing the basis for the possible deactivation of the meteorological water stress scalar [20].

The deactivation of the water stress scalar under irrigated conditions allows accurate prediction of crop $ET_a$ and segmentation of this quantity into water provided by precipitation and irrigation. While the original meteorological scalar represents the rainwater accumulated in the soil and is usable for evapotranspiration, the modified scalar represents this amount supplemented by NIW. As a result, the two scalars can be utilised to minimise the predicted $ET_a$ for rainwater stored in the soil. NIW is calculated from $ET_a$ by considering both the immediate and medium-term effects of precipitation. The former results in a three-day irrigation block—however, the latter accounts for a normalised difference between the modified and original water stress scalars.

This approach requires ground and satellite data affected by relevant uncertainty. The meteorological data are derived from ERA5, which includes daily estimates of ET0 and precipitation. The accuracy of these estimations is determined by both ERA5 and the data obtained for the ground station located in the study area (Tal Amara weather station).

The FVC data are derived from the processing of Sentinel-2 imagery, which provides high spatial resolution (10 m), frequent revisiting time (every 5–10 days), and a standard pre-processed format. This enables the generation of maximum value composite (MVC) images that are only moderately impacted by atmospheric disturbances and have been enhanced further by a multitemporal filtering operation [21]. This study generally confirms the high quality of the radiometrically and atmospherically corrected Sentinel-2 L2A product, which predicts an FVC overestimation during low solar irradiation periods.

A generalised linear equation whose local applicability has been established by Maselli et al. [34] is used to transform NDVI into FVC. Similar estimations could be achieved using the Sentinel Application Platform (SNAP) biophysical processor [22,23], which simulates FVC by using an artificial neural network to analyse multispectral Sentinel-2 images. The current methodology also assumes a uniform maximum Kc for all herbaceous species (1.2), which is the case for potato crops, suggesting that FVC accounts for all Kc variability of annual crops, regardless of type. The low NIW values found for some potato fields in the study area may be attributed to the method's inherent uncertainty, i.e., cases where crop FVC tends to grow throughout the dry season, even without irrigation. The presence of alternate water sources, which increase soil water availability throughout the dry season, could explain these situations.

Regarding the methodology proposed by D'Urso, the results reported in Table 4 indicate that NIW obtained from a P-M equation model with surface resistance modulated using STR is in satisfactory agreement with the measured values from the field. This

finding demonstrates that resistance modulation with OPTRAM accurately reproduces the observed mechanism.

The STR-NDVI space was created using high spatiotemporal resolution Sentinel-2 data, demonstrating dynamic fluctuation between acquisition dates. Agriculture processes like soil moisture change and crop growth development were replicated in dynamic variation. This is especially significant for showing the coevolution of soil moisture and crop growth within irrigated agricultural fields and identifying the critical events and stages of crop growth, as they affect the timing and scheduling of management inputs [35]. Various surface conditions (e.g., irrigated and non-irrigated, bare and vegetated) can be distinguished using dynamic STR-NDVI spaces, and vital agronomic events and crop growth stages (e.g., start and halt of irrigation, crop emergence and maturity, and harvesting time) can be identified. The apparent increase in STR (Figure 8) showed irrigation and the commencement of the growth cycle, but the rise in NDVI and LAI (Figures 5 and 7, respectively) after around 2–4 weeks for both seasons later suggested crop growth. Given the high temporal resolution features of the Sentinel-2 data, it is notable that the coevolution of STR and NDVI reflected by the dynamic STR-NDVI spaces illustrates the overall process of irrigated agriculture in the study area.

Due to low representativeness, a single STR-NDVI space from a single day cannot be utilised to parameterise the wet and dry edges. Although dynamic STR-NDVI spaces, composed of a time series of STR-NDVI spaces, are valuable for assessing the coevolution of surface processes and quantifying spatial heterogeneity, variable potato crop growth status cannot be determined from a single image. To estimate the wet and dry edge parameters, a time series of all photos covering at least a complete growth cycle should generate a complete STR-NDVI space.

Hence, the P-M Sentinel-2 method gives credible estimates of $ET_a$ even in significant water stress. This approach allowed for the characterisation of the potato canopy and provided valuable information for crop management and yield estimation.

The provided dataset, contrasting field-based net irrigation water use (NIW) data with estimations derived from the methodologies of Maselli and D'Urso, reveals a consistent trend of underestimation by both approaches across various seasons. However, the accuracy of these estimation methods in terms of the field-derived data exhibits seasonal variations.

During the early season (represented by fields 1 to 9), both the Maselli and D'Urso methods—(A) and (B), respectively—consistently yield NIW estimates that fall below the actual field measurements. Nevertheless, it appears that, during this phase of crop growth, method (B) tends to approximate the field data more closely than method (A), demonstrating a relatively better accuracy. In contrast, in the late season (fields 10 to 17), the trend of underestimation persists, but the relative accuracy of the methods differs. Here, method (A) tends to provide NIW estimates that better align with the field-derived data, compared to those of method (B).

## 5. Limitations and Further Investigation

Although an acceptable level of soil moisture retrieval accuracy was reached, some significant difficulties regarding the transferability of the OPTRAM technique to other regions remain to be solved and will necessitate future research. The first concern is the availability of data with little or no cloud contamination. It is worth noting that the presented work was carried out in an area where the Sentinel-2 images were mostly cloud-free, allowing for the availability of a high-quality image time series that was well suited for parameterising the trapezoid's dry and wet edges [15]. As a result, high-density Sentinel-2 image time series capturing temporal variations in agricultural growth and irrigation methods were obtained. Several potential solutions to this problem may be applicable: (1) to collect cloud-free images for a more extended period to capture as much detail as possible on crop growth and surface changes; (2) to increase the quality of remote sensing images by refining cloud detection and reduction methods; or (3) to combine Landsat 8-9 with Sentinel-2, considering the availability of SWIR observations in both systems.

Another issue is the model formulation and the edges' parameterisation. The OPTRAM edges can be linear, exponential, or power functions. Thus, strengthening the edge parameterisation using additional formulations has the potential to improve the performance of the OPTRAM approach and the accuracy of soil moisture retrieval [14].

## 6. Conclusions

The use of remote sensing and ancillary data for identifying and quantifying irrigation patterns has been the subject of numerous research efforts over the past few decades [2,35–38]. Most of these studies focus on parametric and nonparametric statistical techniques, which require long, complicated training processes and may have limited generalisation. Additionally, only recent works can fully take advantage of the improved spatio-temporal features of Sentinel-2 imagery data, whereas earlier studies were required to operate at lower spatial resolutions [36].

The current study endeavour is thus unique regarding both the core theory and the spatial and temporal scales of investigation. Both remote sensing-based methods for net irrigation water use (NIW) have distinct advantages and should be considered, based on specific agricultural contexts. One method may excel in certain situations, while the other may offer advantages elsewhere. It is crucial to acknowledge that factors such as soil type, fertiliser application rates, and susceptibility to pests play a significant role in determining the most suitable method. For instance, satellite-based remote sensing can provide broad-scale information over large agricultural regions, making it beneficial for extensive crop monitoring. On the other hand, ground-based remote sensing and sensor networks offer higher spatial and temporal resolution, making them ideal for fine-tuning irrigation management at the field level. A holistic approach, considering both methods and accounting for local variables, including soil conditions and pest pressures, is essential for optimising irrigation practices and maximising agricultural productivity while conserving water resources.

**Supplementary Materials:** The following supporting information can be downloaded at: https://www.mdpi.com/article/10.3390/rs16091598/s1.

**Author Contributions:** Conceptualization and Methodology, G.D. and M.T.A.S.; software and validation, G.M., M.T.A.S., S.R., D.D. and O.R.B.; formal analysis and investigation, G.M., M.T.A.S., S.R., D.D. and O.R.B.; resources, G.D. and M.T.A.S.; data curation, writing—original draft preparation, G.M.; writing—review, editing and supervision, G.D. and M.T.A.S.; project administration, G.D. and D.D.; funding acquisition, G.D. and D.D. All authors have read and agreed to the published version of the manuscript.

**Funding:** This research was funded through ERANETMED EO-TIME (Earth Observation Technologies for Irrigation in Mediterranean Environment), Italian Ministry of University and Research, Decree no.1768/2019, CIHEAM-IAM Bari and by Università di Napoli Federico II, Dipartimento di Agraria, Portici (NA) ITALY.

**Data Availability Statement:** The satellite data used in this study are publicly available at the Copernicus Open Access Hub (https://scihub.copernicus.eu/, accessed on 11 January 2021).

**Conflicts of Interest:** The authors declare no conflicts of interest. The funders had no role in the design of the study, the collection, analysis, or interpretation of data, the writing of the manuscript, or the decision to publish the results.

## Appendix A

**Table A1.** Summary of S-2 A and B images used in the upper Litani watershed study in 2020 season.

| Early Season | | Late Season | |
|---|---|---|---|
| | **Date** | | **Date** |
| S2A | 5 February 2020 | S2A | 4 July 2020 |
| S2A | 16 March 2020 | S2A | 24 July 2020 |

**Table A1.** *Cont.*

| Early Season | | Late Season | |
|---|---|---|---|
| | **Date** | | **Date** |
| S2A | 26 March 2020 | S2A | 3 August 2020 |
| S2A | 15 April 2020 | S2A | 13 August 2020 |
| S2A | 15 May 2020 | S2A | 23 August 2020 |
| S2A | 25 May 2020 | S2A | 2 September 2020 |
| S2A | 4 June 2020 | S2A | 12 September 2020 |
| S2A | 14 June 2020 | S2A | 22 September 2020 |
| S2A | 24 June 2020 | S2A | 2 October 2020 |
| S2A | 4 July 2020 | S2A | 12 October 2020 |
| S2A | 24 July 2020 | S2A | 22 October 2020 |
| S2A | 3 August 2020 | S2A | 1 November 2020 |
| S2A | 13 August 2020 | S2A | 11 December 2020 |
| S2A | 23 August 2020 | S2A | 21 December 2020 |
| | | S2A | 31 December 2020 |
| S2B | 11 March 2020 | S2B | 9 July 2020 |
| S2B | 31 March 2020 | S2B | 19 July 2020 |
| S2B | 20 April 2020 | S2B | 29 July 2020 |
| S2B | 10 May 2020 | S2B | 8 August 2020 |
| S2B | 20 May 2020 | S2B | 18 August 2020 |
| S2B | 30 May 2020 | S2B | 28 August 2020 |
| S2B | 9 June 2020 | S2B | 7 September 2020 |
| S2B | 29 June 2020 | S2B | 17 September 2020 |
| S2B | 9 July 2020 | S2B | 27 September 2020 |
| S2B | 19 July 2020 | S2B | 7 October 2020 |
| S2B | 29 July 2020 | S2B | 17 October 2020 |
| S2B | 8 August 2020 | S2B | 27 October 2020 |
| S2B | 18 August 2020 | S2B | 16 November 2020 |
| S2B | 28 August 2020 | S2B | 26 December 2020 |

## Appendix B

**Table A2.** Characteristics of the multispectral imager (MSI) onboard Sentinel-2 satellites and coefficients for hemispherical albedo calculation.

| Sentinel-2 MSI Spectral Band | Central Wavelength (μm) | Bandwidth (μm) | Exo-Atmosph. Sun Irradiance | Coefficient |
|---|---|---|---|---|
| | | | $E_{sun,\lambda}$ (W m$^{-2}$) | $\omega_\lambda$ |
| 1 | 0.443 | 0.020 | 1893.4 | |
| 2 | 0.490 | 0.065 | 1926.7 | 0.1836 |
| 3 | 0.560 | 0.035 | 1845.7 | 0.1759 |
| 4 | 0.665 | 0.030 | 1528.5 | 0.1457 |
| 5 | 0.705 | 0.015 | 1412.6 | 0.1346 |
| 6 | 0.740 | 0.015 | 1294.4 | 0.1234 |
| 7 | 0.783 | 0.020 | 1189.7 | 0.1134 |
| 8 | 0.842 | 0.115 | 1050.3 | 0.1001 |
| 8a | 0.865 | 0.020 | 970.4 | |
| 9 | 0.945 | 0.020 | 831.0 | |
| 10 | 1.375 | 0.030 | 360.1 | |
| 11 | 1.610 | 0.090 | 242.3 | 0.0231 |
| 12 | 2.190 | 0.180 | 3.0 | 0.0003 |

## References

1. Tilman, D.; Cassman, K.G.; Matson, P.A.; Naylor, R.; Polasky, S. Agricultural sustainability and intensive production practices. *Nature* **2002**, *418*, 671–677. [CrossRef] [PubMed]
2. Ozdogan, M.; Gutman, G. A new methodology to map irrigated areas using multitemporal MODIS and ancillary data: An application example in the continental US. *Remote Sens. Environ.* **2008**, *112*, 3520–3537. [CrossRef]

3. Novelli, F.; Spiegel, H.; Sandén, T.; Vuolo, F. Assimilation of Sentinel-2 Leaf Area Index Data into a Physically Based Crop Growth Model for Yield Estimation. *Agronomy* **2019**, *9*, 255. [CrossRef]
4. Calera, A.; Campos, I.; Osann, A.; D'Urso, G.; Menenti, M. Remote sensing for crop water management: From ET modelling to services for the end users. *Sensors* **2017**, *17*, 1104. [CrossRef] [PubMed]
5. Bausch, W.C. Remote sensing of crop coefficients for improving the irrigation scheduling of corn. *Agric. Water Manag.* **1995**, *27*, 55–68. [CrossRef]
6. D'Urso, G.; Menenti, M.; Santini, A. Regional application of one-dimensional water flow models for irrigation management. *Agric. Water Manag.* **1999**, *40*, 291–302. [CrossRef]
7. Bastiaanssen, W.G.; Molden, D.J.; Makin, I.W. Remote sensing for irrigated agriculture: Examples from research and possible applications. *Agric. Water Manag.* **2000**, *46*, 137–155. [CrossRef]
8. Belmonte, A.C.; Jochum, A.M.; GarcÍa, A.C.; Rodríguez, A.M.; Fuster, P.L. Irrigation management from space: Towards user-friendly products. *Irrig. Drain. Syst.* **2005**, *19*, 337–353. [CrossRef]
9. D'Urso, G.; Richter, K.; Calera, A.; Osann, M.A.; Escadafal, R.; Garatuza-Pajan, J.; Hanich, L.; Perdigão, A.; Tapia, J.B.; Vuolo, F. Earth Observation products for operational irrigation management in the context of the PLEIADeS project. *Agric. Water Manag.* **2010**, *98*, 271–282. [CrossRef]
10. Jensen, M.E.; Burman, R.D.; Allen, R.G. *Evapotranspiration and Irrigation Water Requirements*; FAO: Rome, Italy, 1990.
11. Allen, R.G.; Pereira, L.S.; Raes, D.; Smith, M. *Crop Evapotranspiration—Guidelines for Computing Crop Water Requirements*; FAO Irrigation and Drainage Paper 56; FAO: Rome, Italy, 1998.
12. Ferreira, A.; Rolim, J.; Paredes, P.; Do Rosario Cameira, M. Methodologies for Water Accounting at the Collective Irrigation System Scale Aiming at Optimizing Water Productivity. *Agronomy* **2023**, *13*, 1938. [CrossRef]
13. Garrido-Rubio, J.; González-Piqueras, J.; Campos, I.; Osann, A.; González-Gómez, L.; Calera, A. Remote sensing–based soil water balance for irrigation water accounting at plot and water user association management scale. *Agric. Water Manag.* **2020**, *238*, 106236. [CrossRef]
14. D'Urso, G.; Bolognesi, S.F.; Kustas, W.P.; Knipper, K.R.; Anderson, M.C.; Alsina, M.M.; Hain, C.R.; Alfieri, J.G.; Prueger, J.H.; Gao, F.; et al. Determining Evapotranspiration by Using Combination Equation Models with Sentinel-2 Data and Comparison with Thermal-Based Energy Balance in a California Irrigated Vineyard. *Remote Sens.* **2021**, *13*, 3720. [CrossRef]
15. Sadeghi, M.; Babaeian, E.; Tuller, M.; Jones, S.B. The optical trapezoid model: A novel approach to remote sensing of soil moisture applied to Sentinel-2 and Landsat-8 observations. *Remote Sens. Environ.* **2017**, *198*, 52–68. [CrossRef]
16. Sadeghi, M.; Jones, S.B.; Philpot, W.D. A linear physically based model for remote sensing of soil moisture using short wave infrared bands. *Remote Sens. Environ.* **2015**, *164*, 66–76. [CrossRef]
17. Ambrosone, M.; Matese, A.; Di Gennaro, S.F.; Gioli, B.; Tudoroiu, M.; Genesio, L.; Miglietta, F.; Baronti, S.; Maienza, A.; Ungaro, F.; et al. Retrieving soil moisture in rainfed and irrigated fields using Sentinel-2 observations and a modified OPTRAM approach. *Int. J. Appl. Earth Obs. Geoinf.* **2020**, *89*, 102113. [CrossRef]
18. Maselli, F.; Battista, P.; Chiesi, M.; Rapi, B.; Angeli, L.; Fibbi, L.; Magno, R.; Gozzini, B. Use of Sentinel-2 MSI data to monitor crop irrigation in Mediterranean areas. *Int. J. Appl. Earth Obs. Geoinf.* **2020**, *93*, 102216. [CrossRef]
19. Pelosi, A.; Belfiore, O.R.; D'Urso, G.; Chirico, G.B. Assessing Crop Water Requirement and Yield by Combining ERA5-Land Reanalysis Data with CM-SAF Satellite-Based Radiation Data and Sentinel-2 Satellite Imagery. *Remote Sens.* **2022**, *14*, 6233. [CrossRef]
20. Maselli, F.; Angeli, L.; Chiesi, M.; Fibbi, L.; Rapi, B.; Romani, M.; Sabatini, F.; Battista, P. An improved NDVI-based method to predict actual evapotranspiration of irrigated grasses and crops. *Agric. Water Manag.* **2020**, *233*, 106077. [CrossRef]
21. Maselli, F.; Papale, D.; Chiesi, M.; Matteucci, G.; Angeli, L.; Raschi, A.; Seufert, G. Operational monitoring of daily evapotranspiration by the combination of MODIS NDVI and ground meteorological data: Application and validation in Central Italy. *Remote Sens. Environ.* **2014**, *152*, 279–290. [CrossRef]
22. Vuolo, F.; Żółtak, M.; Pipitone, C.; Zappa, L.; Wenng, H.; Immitzer, M.; Weiss, M.; Baret, F.; Atzberger, C. Data Service Platform for Sentinel-2 Surface Reflectance and Value-Added Products: System Use and Examples. *Remote Sens.* **2016**, *8*, 938. [CrossRef]
23. Weiss, M.; Baret, F. *Sentinel-2 ToolBox Level 2 Products: LAI, FAPAR, FCOVER, Version 1.1*; European Space Agency: Noordwijk, The Netherlands, 2016; Available online: https://step.esa.int/docs/extra/ATBD_S2ToolBox_L2B_V1.1.pdf (accessed on 16 September 2021).
24. Vuolo, F.; D'Urso, G.; De Michele, C.; Bianchi, B.; Cutting, M. Satellite-based irrigation advisory services: A common tool for different experiences from Europe to Australia. *Agric. Water Manag.* **2015**, *147*, 82–95. [CrossRef]
25. Szeicz, G.; Long, I.F. Surface Resistance of Crop Canopies. *Water Resour. Res.* **1969**, *5*, 622–633. [CrossRef]
26. Spank, U.; Köstner, B.; Moderow, U.; Grunwald, T.; Bernhofer, C. Surface Conductance of Five Different Crops Based on 10 Years of Eddy-Covariance Measurements. *Meteorol. Z.* **2016**, *25*, 251–266. [CrossRef]
27. Chávez, J.L.; López-Urrea, R. One-step approach for estimating maize actual water use: Part I. Modeling a variable surface resistance. *Irrig. Sci.* **2019**, *3*, 123–137. [CrossRef]
28. Leuning, R.; Zhang, Y.; Rajaud, A.; Cleugh, H.; Tu, K. A simple surface conductance model to estimate regional evaporation using MODIS leaf area index and the Penman-Monteith equation. *Water Resour. Res.* **2008**, *44*. [CrossRef]
29. Babaeian, E.; Sadeghi, M.; Jones, S.B.; Montzka, C.; Vereecken, H.; Tuller, M. Ground, Proximal, and Satellite Remote Sensing of Soil Moisture. *Rev. Geophys.* **2019**, *57*, 530–616. [CrossRef]

30. Chen, D.; Huang, J.; Jackson, T.J. Vegetation water content estimation for corn and soybeans using spectral indices derived from MODIS near- and short-wave infrared bands. *Remote Sens. Environ.* **2005**, *98*, 225–236. [CrossRef]
31. Feddes, R.; Kabat, P.; Van Bakel, P.; Bronswijk, J.; Halbertsma, J. Modelling soil water dynamics in the unsaturated zone—State of the art. *J. Hydrol.* **1988**, *100*, 69–111. [CrossRef]
32. Weiss, M.; Baret, F.; Jay, S. *S2 ToolBox Level 2 Products: LAI, FAPAR, FCOVER*; Institut National de la Recherche Agronomique (INRA): Avignon, France, 2020; Available online: https://step.esa.int/docs/extra/ATBD_S2ToolBox_V2.0.pdf (accessed on 24 April 2024).
33. West, H.; Quinn, N.; Horswell, M. Remote sensing for drought monitoring & impact assessment: Progress, past challenges and future opportunities. *Remote Sens. Environ.* **2019**, *232*, 111251.
34. Maselli, F.; Angeli, L.; Battista, P.; Fibbi, L.; Gardin, L.; Magno, R.; Rapi, B.; Chiesi, M. Evaluation of MODIS and MSI NDVI data for predicting actual evapo-transpiration in Mediterranean areas. *Int. J. Remote Sens.* **2020**, *41*, 5186–5205. [CrossRef]
35. Zelikova, T.J.; Williams, D.G.; Hoenigman, R.; Blumenthal, D.M.; Morgan, J.A.; Pendall, E. Seasonality of soil moisture mediates responses of ecosystem phenology to elevated $CO_2$ and warming in a semi-arid grassland. *J. Ecol.* **2015**, *103*, 1119–1130. [CrossRef]
36. Chen, Y.; Lu, D.; Luo, L.; Pokhrel, Y.; Deb, K.; Huang, J.; Ran, Y. Detecting irrigation extent, frequency, and timing in a heterogeneous arid agricultural region using MODIS time series, Landsat imagery, and ancillary data. *Remote Sens. Environ.* **2018**, *204*, 197–211. [CrossRef]
37. Ozdogan, M.; Yang, Y.; Allez, G.; Cervantes, C. Remote Sensing of Irrigated Agriculture: Opportunities and Challenges. *Remote Sens.* **2010**, *2*, 2274–2304. [CrossRef]
38. Zaussinger, F.; Dorigo, W.; Gruber, A.; Tarpanelli, A.; Filippucci, P.; Brocca, L. Estimating irrigation water use over the contiguous United States by combining satellite and reanalysis soil moisture data. *Hydrol. Earth Syst. Sci.* **2019**, *23*, 897–923. [CrossRef]